Article

Immunity

Follicular dendritic cells restrict interleukin-4 availability in germinal centers and foster memory B cell generation

Graphical abstract

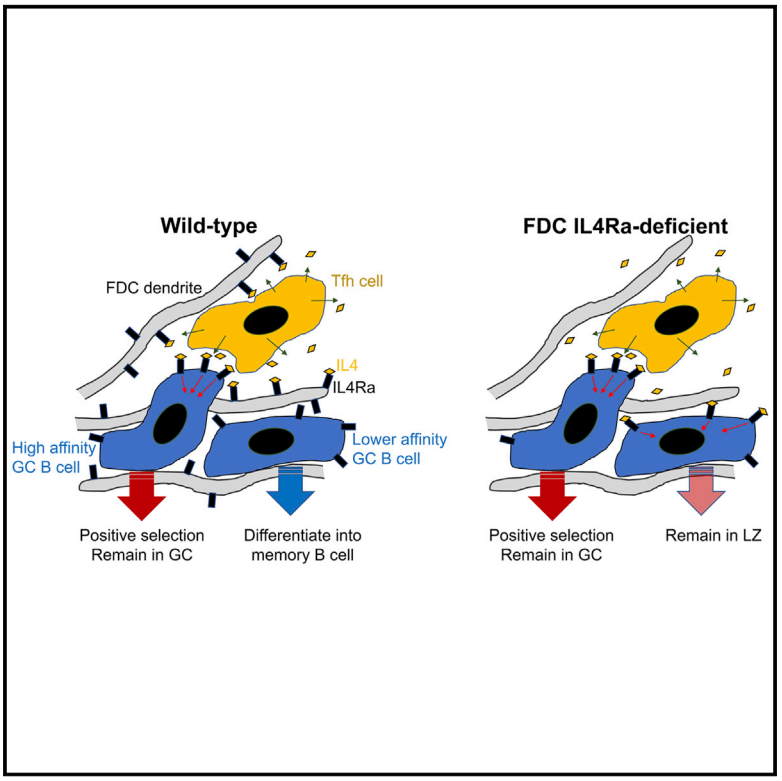

Authors

Lihui Duan, Dan Liu, Hsin Chen, ..., Jinping An, Brian J. Laidlaw, Jason G. Cyster

Correspondence

jason.cyster@ucsf.edu

In brief

B cells within germinal centers (GCs) enter cycles of antibody affinity maturation or exit the GC as memory cells or plasma cells. Duan et al. examine the contribution of interleukin (IL)-4 on B cell fate decisions in the GC and reveal that IL4Ra$^+$ GC follicular dendritic cells limit bystander IL-4 activity, focusing IL-4 action on B cells undergoing selection and enhancing memory cell differentiation.

Highlights

- scRNA-seq identified an IL4Ra$^+$ CD23$^+$ LZ GC B cell subset
- IL-4 restrained CD23$^+$ GC B cell differentiation into memory cells
- IL-4 exerted non-cognate actions within the GC
- FDC IL4Ra restricted GC IL-4 availability and augmented memory B cell generation

Duan et al., 2021, Immunity *54*, 2256–2272
October 12, 2021
https://doi.org/10.1016/j.immuni.2021.08.028

CellPress

CellPress

Immunity

Article

Follicular dendritic cells restrict interleukin-4 availability in germinal centers and foster memory B cell generation

Lihui Duan,[1,3] Dan Liu,[1,3] Hsin Chen,[1,4] Michelle A. Mintz,[1,4] Marissa Y. Chou,[1] Dmitri I. Kotov,[2] Ying Xu,[1] Jinping An,[1] Brian J. Laidlaw,[1,5] and Jason G. Cyster[1,6,*]

[1]Department of Microbiology and Immunology and Howard Hughes Medical Institute, University of California, San Francisco, San Francisco, CA 94143, USA

[2]Division of Immunology and Pathogenesis, Department of Molecular and Cell Biology, and Howard Hughes Medical Institute, University of California, Berkeley, Berkeley, CA 94720, USA

[3]These authors contributed equally

[4]These authors contributed equally

[5]Present address: Division of Allergy and Immunology, Department of Medicine, Washington University School of Medicine, St. Louis, MO, USA

[6]Lead contact

*Correspondence: jason.cyster@ucsf.edu

https://doi.org/10.1016/j.immuni.2021.08.028

SUMMARY

B cells within germinal centers (GCs) enter cycles of antibody affinity maturation or exit the GC as memory cells or plasma cells. Here, we examined the contribution of interleukin (IL)-4 on B cell fate decisions in the GC. Single-cell RNA-sequencing identified a subset of light zone GC B cells expressing high IL-4 receptor-a (IL4Ra) and CD23 and lacking a Myc-associated signature. These cells could differentiate into pre-memory cells. B cell-specific deletion of IL4Ra or STAT6 favored the pre-memory cell trajectory, and provision of exogenous IL-4 in a wild-type context reduced pre-memory cell frequencies. IL-4 acted during antigen-specific interactions but also influenced bystander cells. Deletion of IL4Ra from follicular dendritic cells (FDCs) increased the availability of IL-4 in the GC, impaired the selection of affinity-matured B cells, and reduced memory cell generation. We propose that GC FDCs establish a niche that limits bystander IL-4 activity, focusing IL-4 action on B cells undergoing selection and enhancing memory cell differentiation.

INTRODUCTION

Germinal centers (GCs) are important sites of affinity-based B cell selection (Bannard and Cyster, 2017; MacLennan, 1994; Victora and Nussenzweig, 2012). GCs are divided into a dark zone (DZ) and a light zone (LZ) and GC B cells move cyclically between these compartments. The DZ is composed of proliferating GC B cells that highly express activation-induced-cytidine deaminase (AID) and undergo immunoglobulin (Ig) gene somatic hypermutation. The LZ contains GC B cells and a dense network of follicular dendritic cells (FDCs) that play a crucial role in displaying opsonized antigens to the B cells. The LZ is also the main site for GC B cell interaction with T follicular helper (Tfh) cells. Pre-memory cells are found within the LZ, marked by reduced expression of sphingosine-1-phosphate receptor 2 (S1PR2) and the transcription factor Bcl6 and increased expression of several surface markers, including CCR6 and CD38 (Laidlaw et al., 2017; Suan et al., 2017; Wang et al., 2017). Pre-plasma cells can be found among both LZ and DZ GC cells (Ise et al., 2018; Kräutler et al., 2017; Radtke and Bannard, 2019; Zhang et al., 2018).

GC responses are T cell dependent, and positive selection of GC B cells requires receipt of CD40L signals from Tfh cells. Tfh cells also are an important source of several cytokines, including interleukin (IL)-4. Mice lacking IL-4 or IL4Ra or lacking STAT6, and thus having defective IL4Ra signaling, exhibit strong defects in isotype switching to IgG1 and IgE but variable effects on the GC response, with some studies reporting no effect and others showing a marked defect in the magnitude of the response or a reduction in affinity maturation (Andoh et al., 2000; Chevrier et al., 2017; Cunningham et al., 2004; Gaya et al., 2018; Gonzalez et al., 2018; Reinhardt et al., 2009; Reiter and Pfeffer, 2002; Turqueti-Neves et al., 2014; Vajdy et al., 1995). Deficiency in IL-4 (and IL-13) or in STAT6 can lead to a reduction in the GC LZ relative to the DZ compartment (Gonzalez et al., 2018; Turqueti-Neves et al., 2014).

The magnitude of IL-4 production by Tfh cells is thought to be lower than by Th2-type effector cells and this has been suggested to allow more restricted delivery of IL-4 to cognate partner B cells (Crotty, 2014). However, T cells release IL-4 in a non-directed manner (IL-4 broadcasting), in contrast to the polarized secretion of IL-2 (Huse et al., 2006). In lymph nodes (LNs) responding to a helminth infection, a strong Th2-inducing condition, IL-4 is available non-cognately across the entire LN (Perona-Wright et al., 2010; Turqueti-Neves et al., 2014). These

findings raise the question of whether there are mechanisms that cooperate with low IL-4 production to favor the cognate actions of IL-4 during B cell selection in GCs.

In an earlier single-cell RNA sequencing (scRNA-seq) analyses of stromal cell subsets in lymphoid tissue (Rodda et al., 2018), we found that IL4Ra is expressed in FDCs, raising questions as to whether the IL-4 receptor acts intrinsically in LZ cells and whether FDC IL4Ra could affect cell decision making during this GC stage. We therefore performed experiments to better define how IL-4 acts within the GC. Using droplet-based scRNA-seq, we identified a LZ GC B cell cluster marked by high IL4Ra and CD23 expression and lacking a Myc gene-expression signature. RNA-based cell-fate trajectory and flow cytometry analysis demonstrated that this CD23$^+$ cluster contained pre-memory cells and had the potential to generate pre-plasma cells. scV(D)J-seq revealed that pre-memory cells harbor fewer affinity-improving mutations than pre-plasma cells. IL4Ra and STAT6 functioned intrinsically to promote the CD23$^+$ LZ state and restrained pre-memory B cell generation. This trajectory was dependent on IL-4 availability: the loss of IL4Ra from FDCs was associated with increased IL-4 availability, less stringent affinity-based selection, and reduced memory cell generation. We propose that FDCs provide a niche that limits bystander IL-4 activity, focusing IL-4 action on B cells undergoing selection and enhancing memory B cell generation.

RESULTS

Identification of an IL4Ra$^+$ CD23$^+$ LZ GC B cell subset by scRNA-seq

To obtain insight into the IL-4-responsive B cells within GCs, we performed scRNA-seq on 3,542 GC B cells at day 7 after immunization with 4-hydroxy-3-nitrophenyl (NP)-haptenated antigen (NP-CGG). Clustering analysis led us to identify a subset (cluster 3) of GC B cells that mostly had a LZ gene expression signature and was at the G1 phase of the cell cycle (Figures 1A–1C). A lower depth sequencing analysis of 23,091 cells at day 14 after immunization revealed a greater amount of GC cell heterogeneity but identified an analogous cluster (cluster 1; Figures 1D–1F and S1A). Expression of mRNA for *Il4ra* was enriched in a predominantly LZ cluster, and other distinguishing genes included CD23 (*Fcer2a*), lymphotoxin-b (*Ltb*), *Bank1*, and Gelsolin (*Gsn*) (Figures 1G and 1H; Table S1). Each of these genes is IL-4 inducible in activated B cells (Defrance et al., 1987; Paterson et al., 1996), and CD23 is also inducible in transitional B cells (Granato et al., 2014). For simplicity, we refer to day 7 cluster 3 and day 14 cluster 1 as the CD23$^+$ cluster, although it should be recognized that smaller frequencies of *Fcer2a* high cells were present in some other clusters.

Flow cytometric analysis showed that LZ GC B cells could be divided into CD23$^+$ and CD23$^-$ subsets, while DZ cells were largely CD23$^-$ (Figures 1I and 1J). In accord with the higher *Il4ra* mRNA, the CD23$^+$ subset had higher IL4Ra protein expression (Figure 1K). In agreement with the G1 cell-cycle status designation of the majority of the CD23$^+$ cluster, expression of the cell-cycle-associated marker Ki67 was low in most of these cells (Figure 1L). Flow cytometric analysis showed lower expression of Ki67 protein in CD23$^+$ than CD23$^-$ LZ cells (Figure 1M). One-hour EdU (5-ethynyl-2′-deoxyuridine) labeling confirmed that fewer CD23$^+$ than CD23$^-$ LZ cells were in the cell cycle (Figure 1N). CD23 may also be highly expressed by pre-GC B cells. However, pre-GC B cells are CD38$^+$ and undergo rapid proliferation and show high Ki67 expression (Ise et al., 2018; Schwickert et al., 2009; Wang et al., 2017). The low CD38, low cell-cycle gene expression and low EdU labeling indicated that CD23$^+$ LZ GC B cells were not pre-GC B cells. CD23$^+$ LZ cells were also confirmed to express the definitive GC marker, EprhinB1 (Laidlaw et al., 2017; Wang et al., 2017; Figure 1O). Combined, these data indicate that CD23$^+$ LZ cells have properties that distinguish them from other mature GC B cells.

CD23$^+$ LZ B cells can differentiate into pre-memory and pre-plasma cells

To better understand the difference between clusters of GC B cells, we calculated the score of different gene signatures using VISION (DeTomaso et al., 2019). GC B cells that have recently received strong positive selection signals from Tfh cells are known to be enriched for *Myc* expression and function (Calado et al., 2012; Dominguez-Sola et al., 2012; Ersching et al., 2017; Finkin et al., 2019), and both *Myc* and Myc target genes were more enriched in LZ cells outside of the CD23$^+$ cluster, particularly in cluster 2 (Figures S1B and S1C). In accord with having received T cell help, the populations enriched for Myc$^+$ cells showed a high score for a CD40 signaling gene signature (Figures S1D and S1E) and for hallmark mammalian target of rapamycin complex 1 (mTORC1) signaling (Figure S1F). In addition, hexose kinase-2 (*Hk2*), an enzyme important for glycolysis, was expressed by the Myc$^+$ population, and these cells were enriched for gluconeogenesis pathway activity (Figure S1G). In contrast to the populations enriched for Myc$^+$ cells, CD23$^+$ LZ cells showed enrichment for a B cell receptor (BCR) signaling signature (Figure S1H). These data suggest that this population may have encountered antigen, but not recently had strong cognate interactions with helper T cells. However, there was heterogeneity as can be seen in the upper part of day 7 cluster 3 in the uniform manifold approximation and projection (UMAP) plot where there were some Myc target gene-expressing cells and some S phase cells. Thus, while the cells cluster due to their overall gene expression signature, they were not all in a single state, likely indicating the cluster has multiple outputs.

Previous work has shown that pre-memory and pre-plasma B cells in the GC begin to downregulate the GC marker, S1pr2 (detected using a Venus reporter) (Laidlaw et al., 2017). Flow cytometric analysis showed that the S1pr2-Venus low cells were enriched in the CD23$^+$ compartment (Figures 2A and 2B). Using VISION analysis, the gene expression signature of EphrinB1$^+$ S1pr2^{low} post GC B cells was enriched in the CD23$^+$ cluster (Figures S2A and S2B). The Myc$^+$ cluster also included some cells with post-GC properties (Figure S2A), consistent with some Myc$^+$ cells being pre-plasma cells (Ise et al., 2018). Cluster 5 at day 7 and clusters 8 and 9 at day 14 corresponded to contaminating plasmablasts or plasma cells, and cluster 6 at day 14 corresponded to memory B cells (purity was lower at day 14 because CD38 was not included in the stain).

Applying trajectory inference pseudotime analysis (using Monocle 2; Qiu et al., 2017) to the day 7 (Figures 2C–2E) and day 14 (Figures S2C–S2E) CD23$^+$ cluster LZ cells, we found that these cells could differentiate via two major branches

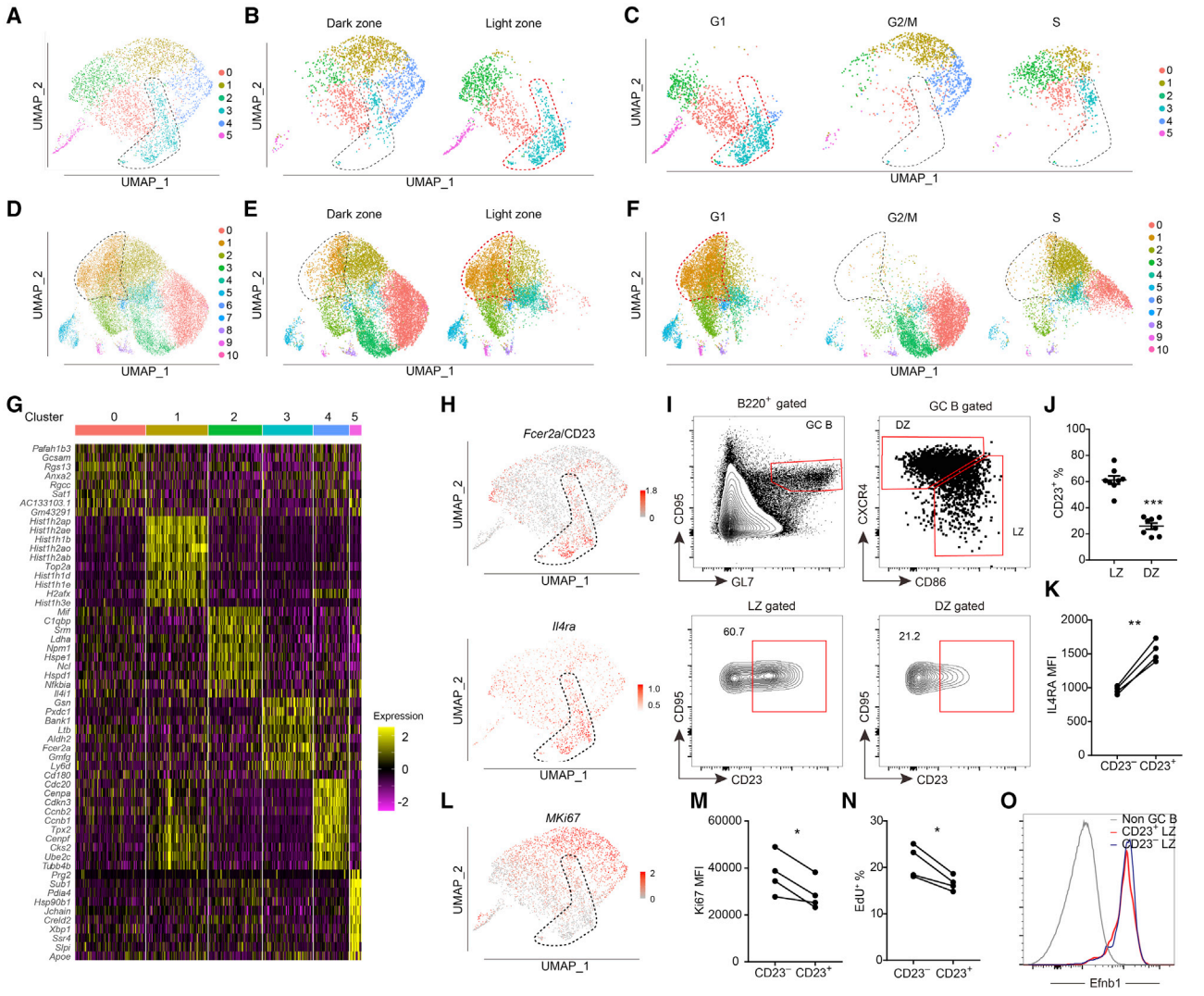

Figure 1. Identification of a CD23$^+$ LZ GC B cell subset by scRNA-seq

(A–C) UMAP plots of sorted B220$^+$ CD38$^-$ GL7^{hi} IgD$^-$ GC B cells at day 7 post-immunization (A), split between LZ and DZ (B) and split among different cell-cycle phases (C).

(D–F) UMAP plots of sorted B220$^+$ CD95^{hi} GL7^{hi} IgD$^-$ GC B cells at day 14 post-immunization (D), split between LZ and DZ (E) and split among different cell-cycle phases (F). Each point is a single cell colored by cluster assignment.

(G) Top 10 marker genes distinguishing the different clusters of GC cells detected at day 7.

(H) Expression of *Fcer2a* (CD23) and *Il4ra* in the day 7 dataset projected onto UMAP plots. Color scaled for each gene with log normalized expression level.

(I and J) Representative fluorescence-activated cell sorting (FACS) profiles (I) and frequencies of CD23$^+$ subset (J) in LZ (CXCR4^{lo} CD86^{hi}) and DZ (CXCR4^{hi} CD86^{lo}) GC B cells 12–14 days after immunization. Each symbol represents 1 mouse. Data are pooled from 2 experiments.

(K) Geometric mean fluorescence intensity (MFI) of IL4Ra in CD23$^-$ and CD23$^+$ LZ GC B cells at day 13 following NP-KLH immunization.

(L) Expression of *Mki67* from day 7 GC B cell dataset projected onto UMAP plots.

(M) MFI of Ki67 in CD23$^-$ and CD23$^+$ LZ GC B cells at day 13 following NP-KLH immunization. One of 2 experiments with a similar result is shown.

(N) Frequencies of EdU$^+$ cells in CD23$^+$ and CD23$^-$ LZ GC B cells after 1-h EdU labeling.

(O) Representative histograms of Efnb1 (Ephrin B1) in non-GC B cells (B220$^+$ CD95^{lo} GL7^{lo}), CD23$^+$, and CD23$^-$ LZ GC B cells 12–14 days after immunization.

In (K), (M), and (N), each symbol represents 1 mouse, each line represents the same mouse, and 1 of 2 experiments with similar results is shown. Data represent 3 experiments, with at least 3 mice per experiment. Data are presented as mean ± SEM; n.s., not significant, *p < 0.05, **p < 0.01, ***p < 0.001.

See also Figure S1 and Table S1.

(Figures 2C and S2C). We compared the differentially expressed genes between these two branches to published pre-memory B cell, pre-plasma cell, and different NP affinity GC B cell RNA-seq datasets (Ise et al., 2018; Shinnakasu et al., 2016; Wang et al., 2017). The highly expressed genes in branch 1 were enriched in the pre-memory B cell signature and also in an NP low-affinity GC B cell signature (Figures 2D, 2E, S2D, and S2E). The genes highly expressed in branch 2 were enriched in the pre-plasma

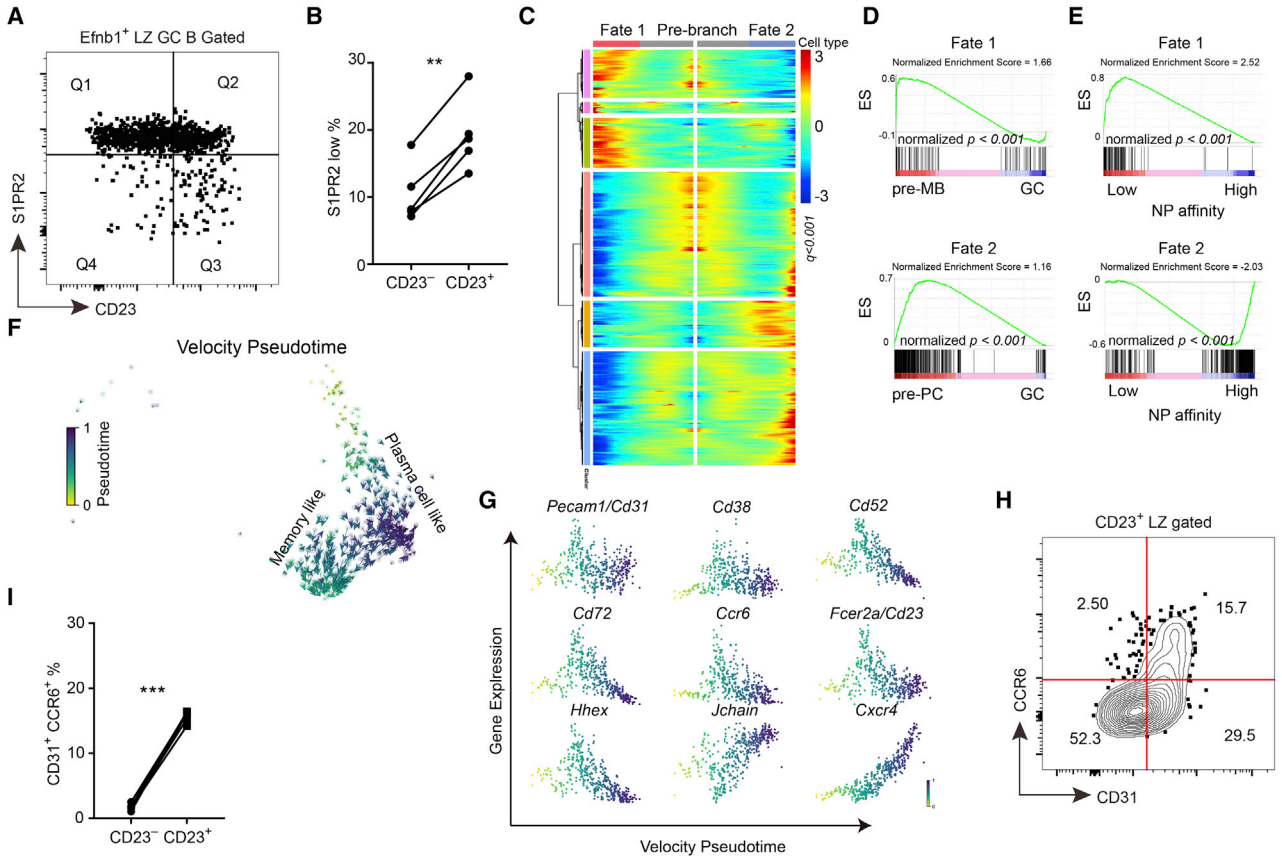

Figure 2. CD23$^+$ LZ B cells can differentiate into pre-memory cells

(A and B) *S1pr2*$^{Venus/+}$ reporter mice were immunized with NP-haptenated antigen.

(A) Representative FACS profile displaying gates between CD23 and S1PR2 in Efnb1$^+$ LZ GC B cells.

(B) Percentages of S1PR2^{lo} cells in CD23$^+$ or CD23$^-$ among Efnb1$^+$ LZ GC B cells. **p < 0.01.

(C) Heatmap of differentially expressed genes between cell fate 1 and cell fate 2 within cluster 3 of day 7 LZ GC B cell dataset by RNA trajectory pseudotime analysis. Colored bars on the side indicate groups of similarly expressed genes (all genes were listed in Table S3).

(D) GSEA analysis of differentially expressed genes from the 2 cell fates compared to pre-memory B cell (Wang et al., 2017) and pre-plasma cell (Ise et al., 2018) RNA-seq datasets. Enrichment profiles for cell fate 1 compared with pre-memory (upper) and cell fate 2 compared with pre-plasma cell (lower).

(E) GSEA of differentially expressed genes from different cell fates compared to RNA-seq dataset of different NP affinity GC B cells (Shinnakasu et al., 2016). Enrichment profiles for cell fate 1 compared with low-affinity (upper) and cell fate 2 compared with high-affinity (lower). ES, enrichment score.

(F) RNA velocity pseudotime analysis for CD23$^+$ LZ GC B cells are embedded in a UMAP plot. Color represents the velocity pseudotime.

(G) Expression level of genes of interest along the velocity pseudotime. Color represents the velocity pseudotime. Determined using scVelo.

(H) Representative FACS profile displaying gates between CD31 and CCR6 in CD23$^+$ LZ GC B cells 12–14 days after immunization. Data are representative of 2 experiments, with at least 3 mice per experiment.

(I) Percentages of CD31$^+$CCR6$^+$ cells in CD23$^-$ and CD23$^+$ LZ GC B cells on day 13 after immunization.

In (B) and (I), each symbol represents 1 mouse, and each line represents the same mouse. ***p < 0.001.

See also Figure S2 and Table S3.

cell and NP high-affinity GC B cell signatures (Figures 2D, 2E, S2D, and S2E). Compared to pre-memory B cells, the cells in branch 2 were more like GC B cells (Figures S2F and S2G). Besides the gene similarity-based pseudotime analysis, we also carried out RNA velocity-based pseudotime analysis (Bergen et al., 2020). Consistent with the previous analysis, CD23$^+$ LZ GC B cells were found to differentiate in two directions (Figure 2F). The markers of pre-memory B cells, which were identified by Monocle 2, were also increased in their expression in one direction (Figure 2G). These cells correspond to the pre-memory cells identified by Monocle 2. By pseudotime analysis, *Ccr6*, *Cd38*, *Cd52*, *Fcer2a* (*Cd23*), *Cd72*, *Pecam1* (*Cd31*), and *Hhex* were upregulated during memory B cell differentiation (Figure 2G). CCR6 and CD38 have been used to identify memory B cell precursors (Laidlaw et al., 2017; Suan et al., 2017), and *Hhex* was recently identified as a key transcription factor for memory B cell formation (Laidlaw et al., 2020). Using antibodies to CCR6 and CD31, a CCR6$^+$CD31$^+$ pre-memory subset could be identified among CD23$^+$ LZ GC B cells (Figure 2H), while there were few such cells among CD23$^-$ LZ GC B cells (Figure 2I). A similar fraction of CD23$^+$CD31$^+$ GC cells stained for the pre-memory marker CD38 (Figure S2H). The pre-memory gene set was also enriched for CD72 and CD31, and CD72 tended to be co-expressed (Figure S2I). IL4Ra expression was also highest on the

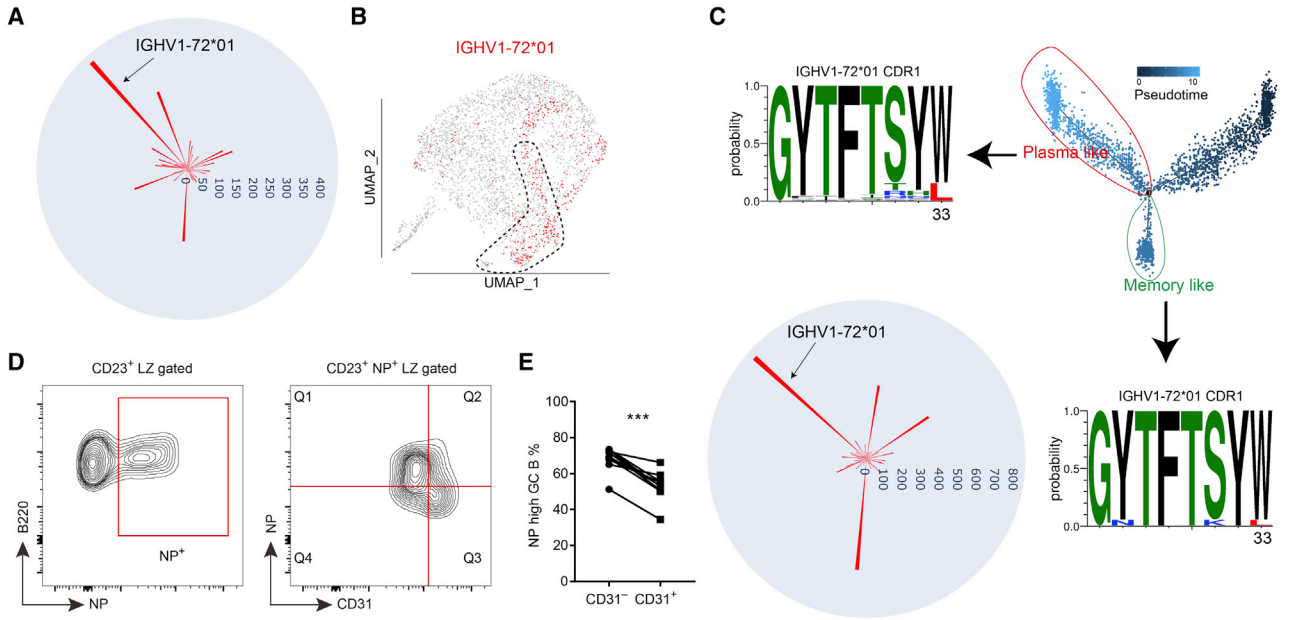

Figure 3. Single-cell VDJ-seq analysis reveals selected heavy-chain gene enrichment in CD23$^+$ LZ cells

(A) Circular bar plot shows the cell number of each heavy-chain gene detected by scVDJ-seq of day 7 GC B cells.

(B) UMAP plot of the distribution of NP specific heavy-chain (IGHV1-72*01) in different clusters of day 7 GC B cells.

(C) Sequence logos of IGHV1-72*01 CDR1 of plasma-like cells and memory-like B cells divided by pseudotime analysis. Circular bar plot shows the cell number of each heavy-chain gene detected by the scVDJ-seq of day 14 GC B cells.

(D and E) Representative FACS profiles (D) and percentages of NP^{hi} subset in CD31$^-$ cells and CD31$^+$ cells among NP$^+$ CD23$^+$ LZ cells 12–14 days after immunization. Each symbol represents 1 mouse, and each line represents the same mouse. Data are pooled from 2 experiments. ***$p < 0.001$.

See also Figure S2.

CD23$^+$CD31$^+$ cells (Figure S2J). In the other branch, CD23$^+$ LZ GC B cells were predicted to differentiate into CD23$^-$ pre-plasma cell-like cells (Figure 2G). Consistent with this prediction, Blimp1-GFP$^+$ cells were enriched in the CD23$^-$ GC B cells (Figures S2K and S2L). By RNA velocity pseudotime analysis, the expression of J chain and CXCR4 were predicted to be upregulated in the pre-plasma cell direction (Figure 2G). CXCR4 upregulation at this early stage is consistent with plasma cells leaving the GC through the DZ (Kräutler et al., 2017; Radtke and Bannard, 2019; Zhang et al., 2018). However, the lack of robust pre-plasma cell surface markers and the late appearance of the Blimp1-GFP reporter during differentiation limited our ability to flow cytometrically quantitate the representation of pre-plasma cells among CD23$^+$ cells compared to other GC subsets from where they may also emerge, and we therefore focused our analysis on memory B cell generation.

scVDJ-seq reveals selected VH gene enrichment in CD23$^+$ LZ cells

To track BCR heavy-chain gene selection and affinity maturation, we performed scVDJ-seq at days 7 and 14 post-NP-haptenated antigen immunization. At the early period after NP immunization, several VH genes are used, but starting from day 6, IGHV1-72*01 (Vh186.2) begins to dominate (Jacob et al., 1993). By scVDJ-seq analysis, IGHV1-72*01 was the most used heavy-chain gene at day 7 (Figure 3A). After mapping the heavy-chain information to the single-cell transcriptome, cells in the CD23$^+$ cluster were enriched for use of IGHV1-72*01 (Figures 3B and S2M). Interestingly, the next two most frequent NP-binding associated VHs, IGHV1-64*01 and IGHV1-53*01 (Jacob et al., 1993), were underrepresented in the CD23$^+$ cluster (Figure S2M), indicating that some feature of IGHV1-72*01 was driving representation in the CD23$^+$ cluster, possibly antigen-binding affinity. Although few mutations of IGHV1-72*01 were detected at day 7, the high NP affinity W33L mutation of IGHV1-72*01 could be detected at day 14 (Figure 3C). By this time point, IGHV1-72*01 was no longer enriched in the CD23$^+$ cluster, and cells carrying the W33L mutation did not show a strong bias for any cluster (Figures S2N and S2O). By pseudotime analysis of the day 14 data, similar to day 7, we could divide the CD23$^+$ cluster into pre-memory-like cells and pre-plasma-like cells (Figures 3C, S2C, and S2D). We next analyzed the scVDJ-seq data in these two subclusters. The W33L mutation was readily detected in the pre-plasma-like cells, while this affinity-improving mutation was rare in pre-memory B cells (Figure 3C). Gene set enrichment analysis (GSEA) also showed that day 14 pre-memory B cells more highly expressed genes enriched in NP low-affinity GC B cells (Figure S2E). Consistent with the sequencing data, 14 days after NP-keyhole limpet hemocyanin (KLH) immunization, CD23$^+$ CD31$^+$ LZ B cells showed lower NP binding than CD23$^+$ CD31$^-$ LZ B cells (Figures 3D and 3E), despite the CD31$^+$ cells having slightly higher total surface BCR levels, as determined by CD79b (Igβ) staining (Figures S2P and S2Q). Lower NP-binding in flow cytometry assays was previously found to be reflective of lower affinity for NP (Shinnakasu et al., 2016). These data demonstrate the ability of

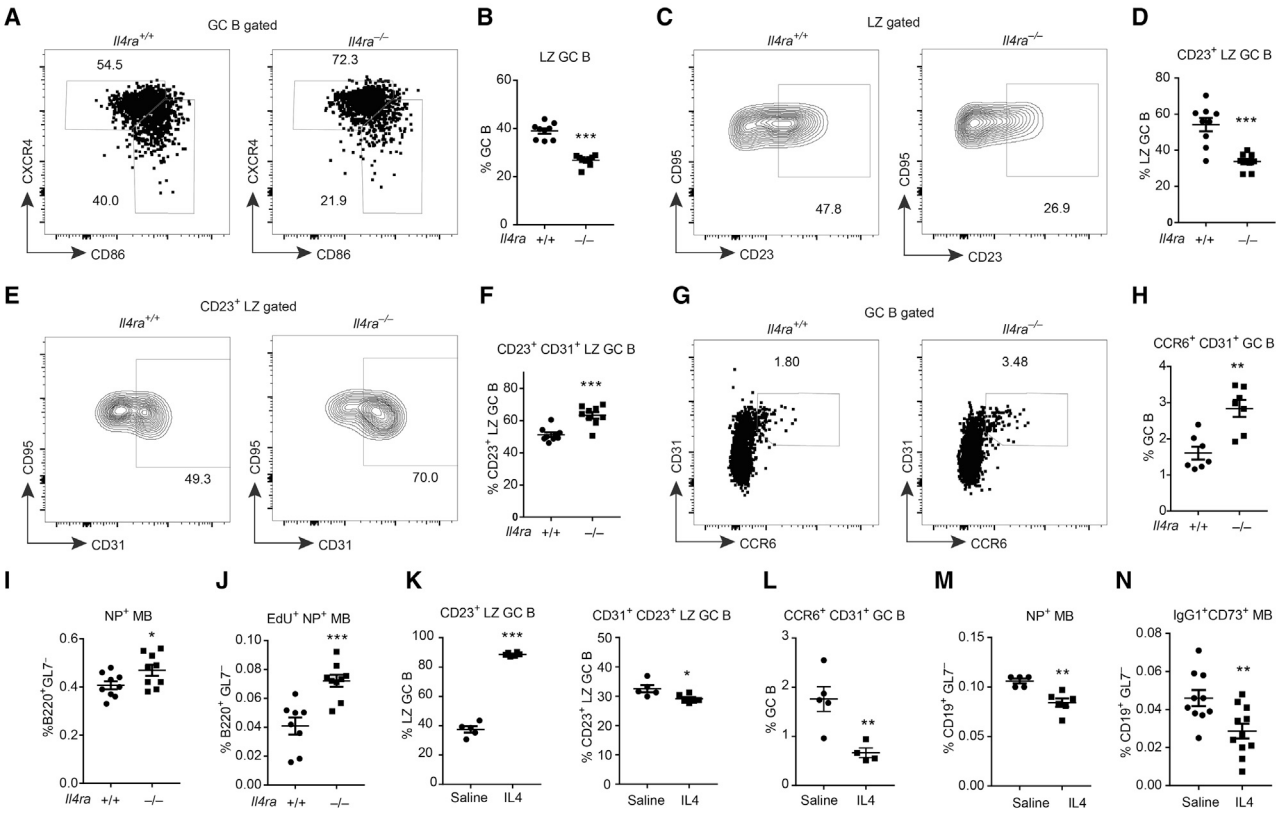

Figure 4. IL4Ra signaling restrains memory B cell development at the CD23$^+$ LZ stage

(A–I) Immunized *Il4ra*$^{+/+}$ and *Il4ra*$^{-/-}$ mice were analyzed on day 13.

(A and B) Representative FACS profiles (A) and frequencies of CXCR4^{lo} CD86^{hi} LZ cells (B) in GC B cells.

(C and D) Representative FACS profiles (C) and frequencies of CD23$^+$ cells (D) in LZ GC B cells.

(E and F) Representative FACS profiles (E) and frequencies of CD31$^+$ cells (F) in CD23$^+$ LZ GC B cells.

(G and H) Representative FACS profiles (G) and frequencies of CD31$^+$ CCR6$^+$ cells (H) in GC B cells.

(I) Frequencies of NP$^+$ memory B cells in B220$^+$ GL7$^-$ non-GC B cells. Data are pooled from 2 experiments.

(J) Immunized *Il4ra*$^{+/+}$ and *Il4ra*$^{-/-}$ mice were treated with EdU on day 11 post-immunization and were analyzed on day 14. Frequencies of NP$^+$ EdU$^+$ memory B cells in B220$^+$ GL7$^-$ non-GC B cells. Data are pooled from 2 experiments.

(K–N) Immunized mice received IL-4-αIL-4 complex or saline on days 11, 12, and 13 post-immunization and were analyzed on day 14.

(K and L) Frequencies of CD23$^+$ cells in LZ GC B cells (K, left), CD31$^+$ cells in CD23$^+$ LZ GC B cells (K, right), and CD31$^+$CCR6$^+$ cells in GC B cells (L).

(M and N) Frequencies of NP$^+$ memory B cells (M) and IgG1$^+$ CD73$^+$ memory B cells (N) in CD19$^+$ GL7$^-$ non-GC B cells. Each symbol represents 1 mouse. (N) Data are pooled from 3 experiments.

(K–M) One of 3 experiments with a similar result is shown. Data are presented as mean ± SEM; *p < 0.05, **p < 0.01, ***p < 0.001.

See also Figure S3.

scRNA-seq to identify and link the early selection and differentiation events of NP-binding GC B cells.

IL4Ra signaling restrains memory B cell development at the CD23$^+$ LZ stage

IL4Ra activation leads to phosphorylation and activation of the transcription factor STAT6 (McCormick and Heller, 2015). Intracellular staining showed that pSTAT6 levels were higher in CD23$^+$ than CD23$^-$ LZ GC B cells (Figure S2R). Moreover, VISION analysis showed a concentration of IL-4 pathway activity in the CD23$^+$ cluster (Figure S2S). Thus, while this cluster has low Myc and mTOR target gene activity, suggesting that the cells are not receiving the strongest levels of T cell help, the IL-4 pathway activity suggests that they are exposed to some helper signals. Lower T cell help could occur due to the presentation of lower amounts of major histocompatibility complex class II (MHC class II)-peptide complexes, leading to less strong triggering of the T cell. In addition, lower T cell help could reflect less cumulative contact time with helper T cells. A further possibility, suggested by data below, is that some B cells could be receiving IL-4 in a non-cognate manner, as bystander cells.

To study the role of IL4Ra signaling in GC LZ cells, *Il4ra*$^{-/-}$ mice were immunized with NP-KLH and analyzed at days 12–14. IL4Ra-deficient mice mounted a GC response of normal magnitude, but there was a 40% reduction in the frequency of LZ cells (Figures 4A, 4B, S3A, and S3B). In accord with the IL4Ra expression data, IL4Ra deficiency caused a preferential depletion of the CD23$^+$ LZ subset (Figures 4C and 4D). Within the CD23$^+$ LZ compartment, however, there was an increased frequency of CD31$^+$ cells (Figures 4E and 4F). In agreement with the CD23$^+$CD31$^+$ cells being enriched for pre-memory B cells, *Il4ra*$^{-/-}$ mice had an increased frequency of CD31$^+$CCR6$^+$

GC B cells (Figures 4G and 4H). *Il4ra*$^{-/-}$ B cells were more competent in memory formation, as there were more B220^{+}GL7^{-}NP^{+} memory cells (Figures 4I, S3C, and S3D). To further test whether these memory cells were GC derived, we injected EdU to label GC B cells at day 11 post-immunization and detected newly generated (EdU-labeled) memory B cells 3 days later. Memory B cell differentiation was significantly increased for *Il4ra*$^{-/-}$ B cells, confirming a role for IL4Ra in restraining memory cell generation (Figure 4J). Measurement of isotype switched cells is also often used to track memory cell generation, but this could not be used for *Il4ra*$^{-/-}$ cells because of the strong defect in IgG1 isotype switching (Figure S3E). In addition to the effects on memory B cell generation, there was also a small increase in the abundance of IgD^{-}CD138^{+} plasma cells in *Il4ra*$^{-/-}$ mice (Figures S3F and S3G).

To investigate whether IL-4 was sufficient to restrain memory B cell differentiation *in vivo*, we treated mice with IL-4-αIL-4 complexes (Finkelman et al., 1993; Ricardo-Gonzalez et al., 2010) for 3 days starting at day 11. The frequency of GC B cells was not changed by the treatment (Figure S3H), but the frequency of IgG1^{+} GC B cells was increased (Figure S3I). The frequency of LZ cells and CD23^{+} LZ cells was markedly increased (Figures 4K and S3J). The percentages of CD23^{+}CD31^{+} LZ B cells (Figure 4K) and CCR6^{+}CD31^{+} pre-memory cells (Figure 4L) were significantly reduced. Similar reductions were noted for NP^{+} memory B cells (Figure 4M). CD73 is a marker of many, although not all, memory B cells, and it can be differentially induced depending on immunization conditions, with some studies indicating it is preferentially expressed on memory cells generated in a Bcl6-dependent manner (Anderson et al., 2007; Bemark et al., 2016; He et al., 2017; Kaji et al., 2012; Onodera et al., 2012; Taylor et al., 2012; Tomayko et al., 2010). We also gated IgG1^{+}CD73^{+} memory cells and found that their frequency among CD19^{+}GL7^{-} cells was reduced (Figures 4N and S3K), even though the overall amount of B cell IgG1 switching was increased (Figure S3I). The frequency of plasma cell was also reduced following IL-4-αIL-4 complex treatment (Figure S3L). These data suggest that IL-4 is sufficient to restrain GC B cell differentiation from a CD23^{+} LZ state to the memory state and that it may also restrain plasma cell generation. In keeping with these findings, previous *in vitro* work has shown that IL-4 pathway activity can restrict plasma cell differentiation (Ettinger et al., 2005; Jenks et al., 2018; Pignarre et al., 2021).

Memory B cell differentiation can be affected by BCR affinity and/or Ig class switch (Gitlin et al., 2016; Viant et al., 2020). To investigate whether the repression effect of IL-4 on memory cell generation was caused by affinity and/or class switch modulation, we treated AID-deficient mice with IL-4-αIL-4 complexes for 3 days starting at day 11. Similar to the wild-type mice, IL-4 treatment caused a reduction in differentiation of memory B cells (Figures S3M–S3P). These data suggest that IL-4 restrains memory B cell differentiation independently of effects on BCR affinity or class switch.

In agreement with a repressive action of IL-4 on memory B cell development, an analysis of published B cell RNA-seq data (Mokada-Gopal et al., 2017) revealed that *in vitro* incubation of follicular B cells with IL-4 inhibits the expression of many markers expressed by memory B cells such as *Cd31*, *Cd38*, *Cd72*, *Ccr6*, and *Cr2* and the memory B cell differentiation-related transcription factors *Hhex*, *Bach2*, and *Zbtb32*, while promoting expression of *Fcer2a and Il4ra* (Figure S3Q). This regulation of gene expression could be released by the deletion of *Stat6* (Figure S3Q).

IL4Ra acts intrinsically in GC B cells

To determine whether the increased predisposition of GC B cells to a memory cell fate in the absence of IL4Ra was due to a cell-intrinsic role of the receptor, we generated wild-type (WT) CD45.1 and WT or *Il4ra*$^{-/-}$ CD45.2 mixed bone marrow (BM) chimeras. The influence of IL4Ra deficiency on B cell representation in a particular stage of the GC response was determined by comparing the ratio of CD45.2^{+} (WT or *Il4ra*$^{-/-}$, depending on the chimera) to CD45.1^{+} (WT) B cells in the target population (e.g., LZ) with the corresponding ratio in the parent population for that subset (total GC in the LZ case) to obtain a competency measurement (Figures S4A–S4C). Thus, if *Il4ra*$^{-/-}$ cells were present at a ratio of 3:1 in the target population but had been 2:1 in the parent population, then the competency measurement would be 1.5. This method allows standardization across different sets of mice that had different levels of hematopoietic chimerism. The chimeric mice showed a notable underrepresentation of *Il4ra*$^{-/-}$ B cells in the GC (Figures S4C and S4D), likely due to lower competitiveness of these cells for expansion in the pre-GC compartment. We also noted a reduction in the frequency of total GC cells in the WT:*Il4ra*$^{-/-}$ mixed chimeras compared to the control mixed chimeras (Figure S4E). These findings were unexpected given the unaltered GC response magnitude in the full *Il4ra*$^{-/-}$ mice (Figure S3B) and suggest complex interactions between WT and *Il4ra*$^{-/-}$ cells that we dissect further in later experiments.

In the mixed chimeras, IL4Ra-deficient B cells showed a disadvantage in total LZ and CD23^{+} LZ (Figure 5A) but showed an advantage in the CD23^{+}CD31^{+} and CD31^{+}CCR6^{+} pre-memory compartment (Figures 5A, 5B, and S4F). Assessment of the effect of IL4Ra deficiency on the memory compartment in the mixed chimeras was problematic because of the low representation of *Il4ra*$^{-/-}$ cells in GCs and our lack of a definitive marker for GC-derived memory cells. Interestingly, when we examined the behavior of CD45.1 WT cells in GCs containing ~50% *Il4ra*$^{-/-}$ CD45.2 cells, we noted that there were reductions in the frequencies of CD23^{+}CD31^{+} and CD31^{+}CCR6^{+} WT cells compared to their representation in GCs composed of only WT cells (Figure 5B, black symbols; CD45.2 WT or *Il4ra*$^{-/-}$ cells shown in red symbols). A reduction in WT CD23^{+}CD31^{+} and CD31^{+}CCR6^{+} cells was also seen after IL-4 injection (Figures 4K and 4L) and could be occurring in the WT:*Il4ra*$^{-/-}$ mixed chimeras due to reduced IL-4 consumption by *Il4ra*$^{-/-}$ GC cells leading to increased IL-4 availability for WT cells. In agreement with the idea of a general increase in splenic IL-4 availability, the WT cells in WT:*Il4ra*$^{-/-}$ mixed chimeras showed an increased extent of switching to the IL-4-dependent IgG1 isotype compared to cells in WT:WT mixed chimeras (Figure 5C).

An analogous assessment of WT:*Stat6*$^{-/-}$ mixed BM chimeras showed a similar advantage of *Stat6*$^{-/-}$ cells in the CD23^{+}CD31^{+} LZ subset (Figure 5D). Importantly, however, these mixed chimeras did not show the disadvantage of CD23^{+}CD31^{+} WT cells competing with the *Stat6*$^{-/-}$ cells (Figure 5E). Stat6 deficiency did not alter the IL4Ra surface levels on GC B cells (Figure S4G),

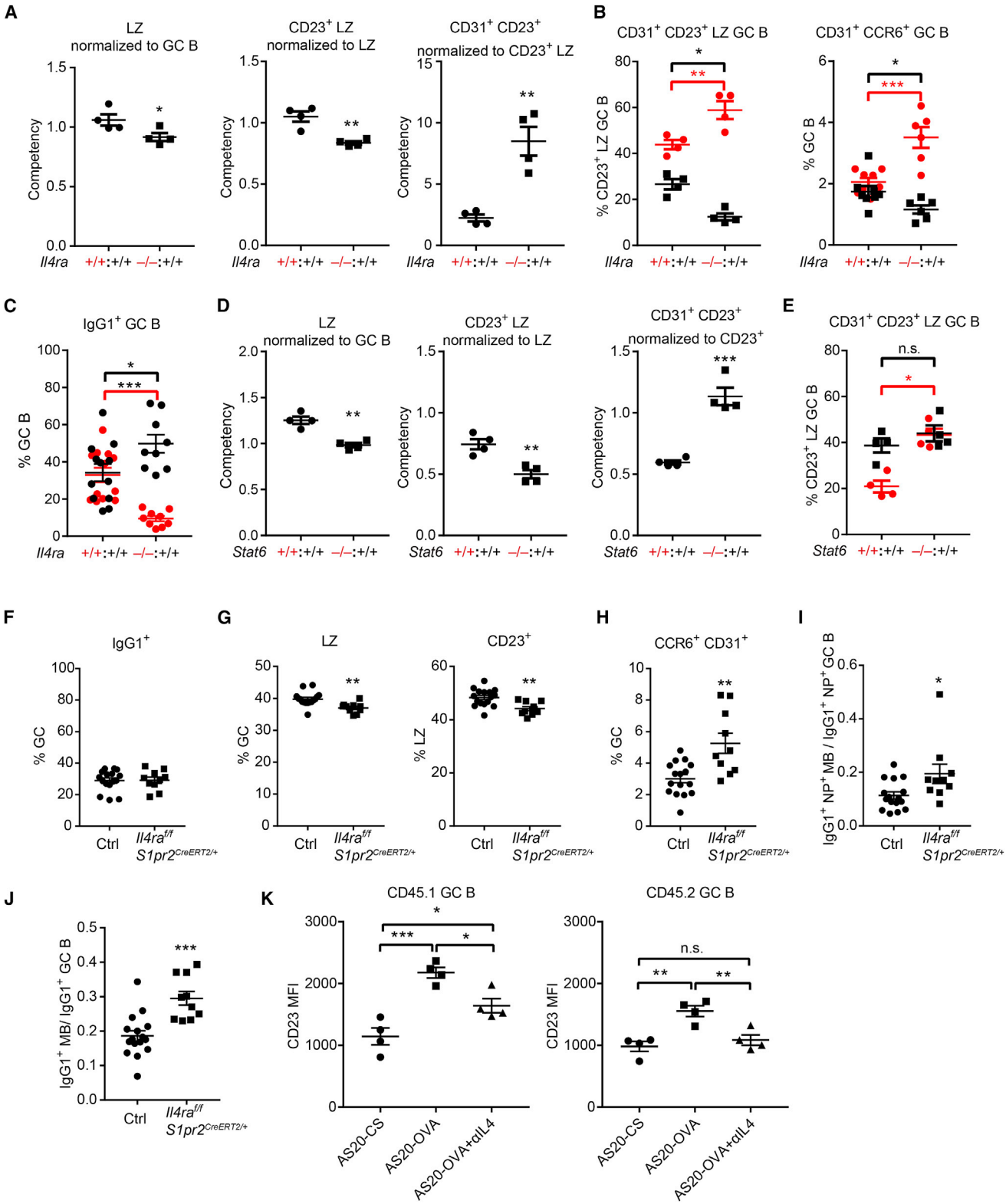

Figure 5. IL4RA and STAT6 are intrinsically required for restraining memory B cell development

(A–C) Mixed BM chimeras were made with CD45.1 wild-type (*Il4ra*$^{+/+}$) and CD45.2 *Il4ra*$^{+/+}$ or *Il4ra*$^{-/-}$ BM cells. (A and B) One of 3 experiments with similar results is shown.

(legend continued on next page)

and there was no increase in IgG1$^+$ WT GC B cells in the WT:*Stat6*$^{-/-}$ mixed chimeras (Figure S4H). Therefore, we speculate that in contrast to the situation in *Il4ra*$^{-/-}$ mixed BM chimeras, the IL-4 available in the lymphoid tissue microenvironment to WT cells is unlikely to be changed in *Stat6*$^{-/-}$ mixed BM chimeras.

Besides Stat6, IL-4 could also signal via insulin receptor substrate1/2 (IRS1/2) (Wills-Karp and Finkelman, 2008). To further investigate the Stat6 dependence of IL-4 signaling in the GC, we treated Stat6-deficient mice with IL-4 complexes for 3 days starting 11 days after immunization. Although IL-4 could still slightly increase the percentage of LZ cells and the expression of CD23, the frequency of CCR6$^+$CD31$^+$ GC B cells and memory B cells was not altered (Figures S4I and S4J), indicating that IL-4 signaling via STAT6 is needed for effects on memory cell generation.

Our studies in WT:*Il4ra*$^{-/-}$ mixed BM chimeras could not exclude the possibility that the influence of IL4Ra deficiency on memory cell generation was due to effects occurring before GC formation. We took two approaches to address this issue. First, we reconstituted mice with *Cγ1*$^{Cre/+}$ *Cas9*$^{f/+}$ BM that had been transduced with single-guide RNA (sgRNA) against IL4Ra (using a vector containing a blue fluorescent protein [BFP] reporter) (Figure S5A). This approach achieved knockdown of IL4Ra in many BFP$^+$ GC B cells and was associated with a reduction in the LZ compartment and an increase in the frequency of CCR6$^+$CD31$^+$ pre-memory cells among BFP$^+$ GC cells (Figure S5B). The frequency of IgG1$^+$ cells among BFP$^+$ GC cells was unchanged compared to BFP$^-$ GC cells (Figure S5C). Comparing the frequency of IgG1$^+$CD38$^+$ memory B cells with IgG1$^+$ GC B cells or the frequency of NP$^+$CD38$^+$ memory B cells with NP$^+$ GC B cells showed that the conditional loss of IL4Ra was associated with an increase in memory cell generation (Figures S5D and S5E). However, Cγ1Cre is expressed in some activated B cells as well as in GC B cells and thus does not strictly limit the IL4Ra knockdown to the GC stage. Second, we generated *S1pr2*$^{CreERT2/+}$*Il4ra*$^{f/f}$ mice and treated them early after immunization with tamoxifen to induce selective ablation of IL4Ra in GC B cells. This approach caused a reduction in IL4Ra in ~50% of GC B cells without altering expression in follicular B cells (Figure S5F). Interestingly, as in the WT:*Il4ra*$^{-/-}$ BM chimeras (Figure S4E), but not full *Il4ra*$^{-/-}$ mice (Figure S3B), these mice showed a reduction in the magnitude of the overall GC response (Figure S5G). The conditional IL4Ra-deficient mice showed unaltered frequencies of IgG1$^+$ cells among GC cells (Figure 5F). The LZ and CD23$^+$ LZ were reduced, while the CCR6$^+$CD31$^+$ pre-memory cells were increased (Figures 5G and 5H). In reference to IgG1$^+$NP$^+$ GC cells to control for the smaller GC size, there was an increased proportion of IgG1$^+$NP$^+$ CD38$^+$ memory B cells; this increase was also seen for total IgG1$^+$ memory B cells (Figures 5I and 5J). These data indicate that intrinsic IL4Ra signaling within GC B cells restrains the extent of pre-memory and memory B cell generation.

Another notable feature of the CD23$^+$ GC B cells was their higher expression of *Lt*α and *Lt*β than most other GC B cells (Figures 1G and S5H). Flow cytometric analysis with LTβR-Ig confirmed that CD23$^+$ LZ GC B cells had higher LTα1β2 expression than total GC B cells (Figures S5I and S5J). Moreover, IL4Ra and Stat6 were intrinsically required for normal Lα1β2 expression in GC B cells (Figures S5K–S5N). These findings are in accord with the activity of IL-4 in promoting LTα1β2 expression in B and T lymphocytes (Cortes-Selva et al., 2019; Dubey et al., 2017; Luther et al., 2002). GC FDCs are strongly dependent on LTα1β2 for their maintenance (Fu and Chaplin, 1999; Haberman et al., 2019; Mackay and Browning, 1998). Therefore, the extent of IL-4 signaling in CD23$^+$ GC B cells may influence properties of the GC FDC network.

Non-cognate IL-4 actions in the GC

Findings in the WT:*Il4ra*$^{-/-}$ mixed BM chimeras provided evidence for bystander actions of IL-4 in the GC. As a further test for possible non-cognate actions of IL-4 in the GC, we asked whether augmenting the delivery of T cell help to a subset of GC B cells would lead to evidence of increased IL-4 signaling in bystander GC B cells. Following a similar strategy to the DEC205-OVA (ovalbumin) method for antigen loading of B cells independently from the BCR (Victora et al., 2010), we coupled OVA to the AS20 (A20-1.7) antibody that is specific for CD45.1. Adoptive transfers were performed with 10:90 mixtures of CD45.1 MD4 and CD45.2 MD4 hen egg lysozyme (HEL)-specific B cells together with OVA-specific OT2 T cells into CD45.2 recipients. After immunizing with HEL-OVA to establish a GC

(A) Competency values of LZ (B220$^+$ CD95^{hi} GL7^{hi} CXCR4^{lo} CD86^{hi}) (left), CD23$^+$ LZ (center), and CD31$^+$ CD23$^+$ LZ (right) GC compartment at day 13 following immunization.
(B) Frequencies of CD31$^+$ cells in CD23$^+$ LZ GC B cells (left) and CCR6$^+$ CD31$^+$ cells in GC B cells (right) in different compartments (black CD45.1$^+$ and red CD45.2$^+$) of mixed chimeras.
(C) Frequencies of IgG1$^+$ cells in GC B cells in different compartments (black CD45.1$^+$ and red CD45.2$^+$) of mixed chimeras. Gating strategy and equation for calculating differentiation ratios shown in Figures S4A–S4C. Data are pooled from 3 experiments.
(D and E) Mixed (50:50) BM chimeras were made with CD45.1 wild-type (*Stat6*$^{+/+}$) and CD45.2 *Stat6*$^{+/+}$ or *Stat6*$^{-/-}$ BM cells.
(D) Competency values of LZ (left), CD23$^+$ LZ (center), and CD31$^+$ CD23$^+$ LZ (right) GC compartment at day 13 following immunization.
(E) Frequencies of CD31$^+$ cells in CD23$^+$ LZ GC B cells in different compartments (black CD45.1$^+$ and red CD45.2$^+$) of mixed chimeras. One of 2 experiments with similar results is shown.
(F–J) Control and *S1pr2*$^{CreERT2/+}$ *Il4ra*$^{f/f}$ mice were immunized with NP-KLH, treated with tamoxifen to induce Cre expression, and analyzed on day 13.
(F) Frequencies of IgG1$^+$ cells in GC B cells.
(G and H) Frequencies of LZ cells in GC B cells (G, left), CD23$^+$ cells in LZ GC B cells (G, right), CD31$^+$CCR6$^+$ cells in GC B cells (H).
(I) Ratio of NP$^+$ IgG1$^+$ memory B cells to NP$^+$IgG1$^+$ GC B cells.
(J) Ratio of CD38$^+$IgG1$^+$ memory B cells to CD38$^-$IgG1$^+$ GC B cells. Data are pooled from 3 experiments.
(K) Geometric MFI of CD23 in CD45.1$^+$ (left) and CD45.2$^+$ MD4 GC B cells with indicated treatment. One of 2 experiments with similar results is shown. In (K), one-way ANOVA with Sidak multiple comparisons test was used.
In all of the plots, each symbol represents 1 mouse. Data are presented as mean ± SEM; *p < 0.05, **p < 0.01, ***p < 0.001.
See also Figures S5 and S6.

response, the mice were treated with AS20-OVA (Figure S5O). The treatment led to expansion of the OVA-loaded (CD45.1) MD4 B cells in the LZ at 12 h and in the DZ at 72 h (Figures S5P and S5Q). These findings are comparable to those observed with the DEC205-OVA-based GC B cell antigen-loading system (Victora et al., 2010) and they establish a versatile method for differential antigen loading *in vivo* using widely available CD45 congenic mice. Using this cell transfer and antigen-loading approach, we tested for cognate and non-cognate influences of T cells on CD23 expression after 12 h. In these experiments, we transferred 80:20 mixtures of CD45.1 MD4 and CD45.2 MD4 cells. The antigen-loaded CD45.1 MD4 GC B cells showed a strong increase in CD23, consistent with cognate receipt of CD40 and IL-4 signals; importantly, the bystander CD45.2 GC B cells also showed a measurable increase in CD23 (Figure 5K). The bystander increase in CD23 was fully blocked by treatment with anti-IL-4 (Figure 5K). These data indicate that under conditions in which many GC B cells are interacting strongly with Tfh cells, bystander GC B cells can be exposed to IL-4.

Searching for an explanation for the reduced GC magnitude in WT:*Il4ra*$^{-/-}$ BM chimeras and tamoxifen-treated *S1pr2*$^{CreERT2/+}$ *Il4ra*$^{f/f}$ mice (also chimeric in their IL4Ra loss) versus the intact GC response in *Il4ra*$^{-/-}$ mice, we considered the possibility that in the mixed setting, the chronically elevated available IL-4 was having a repressive influence on the WT GC cells. In accordance with this notion, when mice were treated with IL-4 complexes daily for 3 days, their GC B cells showed lower Bcl6 protein levels (Figure S5R); by contrast, Bcl6 was increased in follicular B cells, in keeping with *in vitro* findings for activated B cells (Chevrier et al., 2017; Haniuda et al., 2020; Robinson et al., 2019). Moreover, by the fourth day of IL-4 complex treatment, there was a reduction in the magnitude of the GC response (Figure S5S). *In vitro* studies have shown that under some conditions, IL-4 can suppress B cell proliferation or promote apoptosis (Jelinek and Lipsky, 1988; Pignarre et al., 2021). These findings further highlight the importance of appropriately controlled IL-4 signaling during the GC response.

IL4Ra expression by FDCs limits IL-4 availability to GC B cells

scRNA-seq data of LN and spleen stromal cells (Cheng et al., 2019; Rodda et al., 2018) showed that IL4Ra was expressed by FDCs but not other types of fibroblastic reticular cells (Figures 6A and S6A). During this analysis, we also found that epithelial cell adhesion molecule (*Epcam*) is specifically expressed by FDCs (Figures 6A and S6A). Co-staining Epcam with the FDC markers Cr2 and Tmem119 in tissue sections confirmed the selective expression of this adhesion molecule by FDCs (Figures S6B and S6C). Combining Epcam with CR2 (CD21) staining in flow cytometry allowed for improved identification of FDCs (Figure 6B). Consistent with the scRNA-seq data, ILR4a was selectively expressed on FDCs by flow cytometry (Figure 6C).

In an effort to determine whether the IL4Ra expressed by FDCs affects the GC response, we generated reverse BM chimeric mice that lacked IL4Ra on all radiation-resistant cells, but had intact expression on B cells, T cells, and other hematopoietic cells. Immunized *Il4ra*$^{-/-}$ reverse BM chimeras revealed a normal frequency of GC B cells (Figure 6D) and of FDCs (Figure S6D), but had an increased frequency of LZ GC B cells (Figure 6E). Among the LZ cells, there was a higher percentage of CD23^{+} cells and a lower percentage of CD31^{+} cells in the CD23^{+} LZ compartment (Figure 6E). The fraction of GC cells that switched to IgG1 was increased (Figure 6F). In these experiments, a lower valency form of the immunogen (NP14-CGG) was used than in other experiments (in which NP28-CGG, NP28-KLH, or NP32-KLH was used), and this was associated with a weaker NP-specific response that precluded quantitating NP^{+} memory B cells. However, compared to the overall frequency of IgG1^{+} cells, there was a reduction in IgG1^{+}CD73^{+} memory cells (Figure 6G). Plasma cell frequencies were also down (Figure S6E). To determine whether signaling via the IL-4 receptor was important in stromal cells, we also studied BM chimeras lacking the cytokine cγ chain that is needed for IL4R signaling (McCormick and Heller, 2015) and was also expressed by FDCs (Figure S6F). In these animals, there was no significant difference in GC, LZ, memory, or plasma cell compartments (Figures S6G–S6L). IL-4 can also signal via the IL4Ra/IL13Ra complex (McCormick and Heller, 2015). We detected minimal IL13Ra expression by FDCs (Figure S6M), making it unlikely that this complex is involved in FDC responses to IL-4, although our data do not fully exclude this possibility.

Given the widespread expression of IL4Ra by tissue cell types, it was important to perform more restricted deletion of IL4Ra. We took advantage of *Ccl19*$^{Cre/+}$ to restrict IL4Ra deletion to lymphoid stromal cells, including FDCs (Cheng et al., 2019) and of *CD21*$^{Cre/+}$ to restrict ablation to FDCs among stromal cells (Kraus et al., 2004; Wang et al., 2014). In the latter animals, ablation also occurs in B cells, but expression here was rescued by studying irradiated mice that have been reconstituted with WT BM. Unexpectedly, we found that *Ccl19*$^{Cre/+}$ led to the deletion of IL4Ra in a fraction of B cells and we therefore also reconstituted these mice with WT BM before performing the immunizations. Staining of spleen sections for CD35 (CR1) showed that the GC FDC networks were comparable between control and *Ccl19*$^{Cre/+}$ *Il4ra*$^{f/f}$ chimeras (Figure S6N). In contrast to the full *Il4ra*$^{-/-}$ BM chimeras, IgG1^{+} GC cell frequencies were not increased in either the *CD21*$^{Cre/+}$ *Il4ra*$^{f/f}$ chimeras (Figures 6H and 6I) or the *Ccl19*$^{Cre/+}$ *Il4ra*$^{f/f}$ chimeras (Figures S6O and S6P). Importantly, however, in both the *CD21*$^{Cre/+}$ *Il4ra*$^{f/f}$ chimeras (Figure 6J and 6K) and the *Ccl19*$^{Cre/+}$ *Il4ra*$^{f/f}$ chimeras (Figures S6Q and S6R), there was an increase in the CD23^{+} LZ, a decrease in CD31^{+}CD23^{+} cells within the CD23^{+} LZ compartment, and a decrease in CD31^{+}CCR6^{+} pre-memory cells. There was also a decrease in NP^{+} and CD73^{+} IgG1^{+} memory B cells (Figures 6L, 6M, and S6S). When considered together with the above findings for IL-4-treated mice and mice lacking IL4Ra on some GC B cells (Figures 4K–4N and 5B), it can be suggested that the abundance of IL-4 in the GC is increased when stromal cells lack IL4Ra. To account for the differential effects on IgG1 switching, we speculate that in mice lacking IL4Ra on all non-hematopoietic cells, IL-4 availability is widely increased, including in pre-GC niches where isotype switching occurs, as well as within GCs; when IL4Ra loss is restricted to FDCs, IL-4 availability may only be increased in the GC, a microenvironment where little, if any, isotype switching occurs (Roco et al., 2019; Sundling et al., 2021).

To further test the impact of stromal IL4Ra deficiency on the memory B cell compartment, immunized *Ccl19*$^{Cre/+}$ *Il4ra*$^{f/f}$

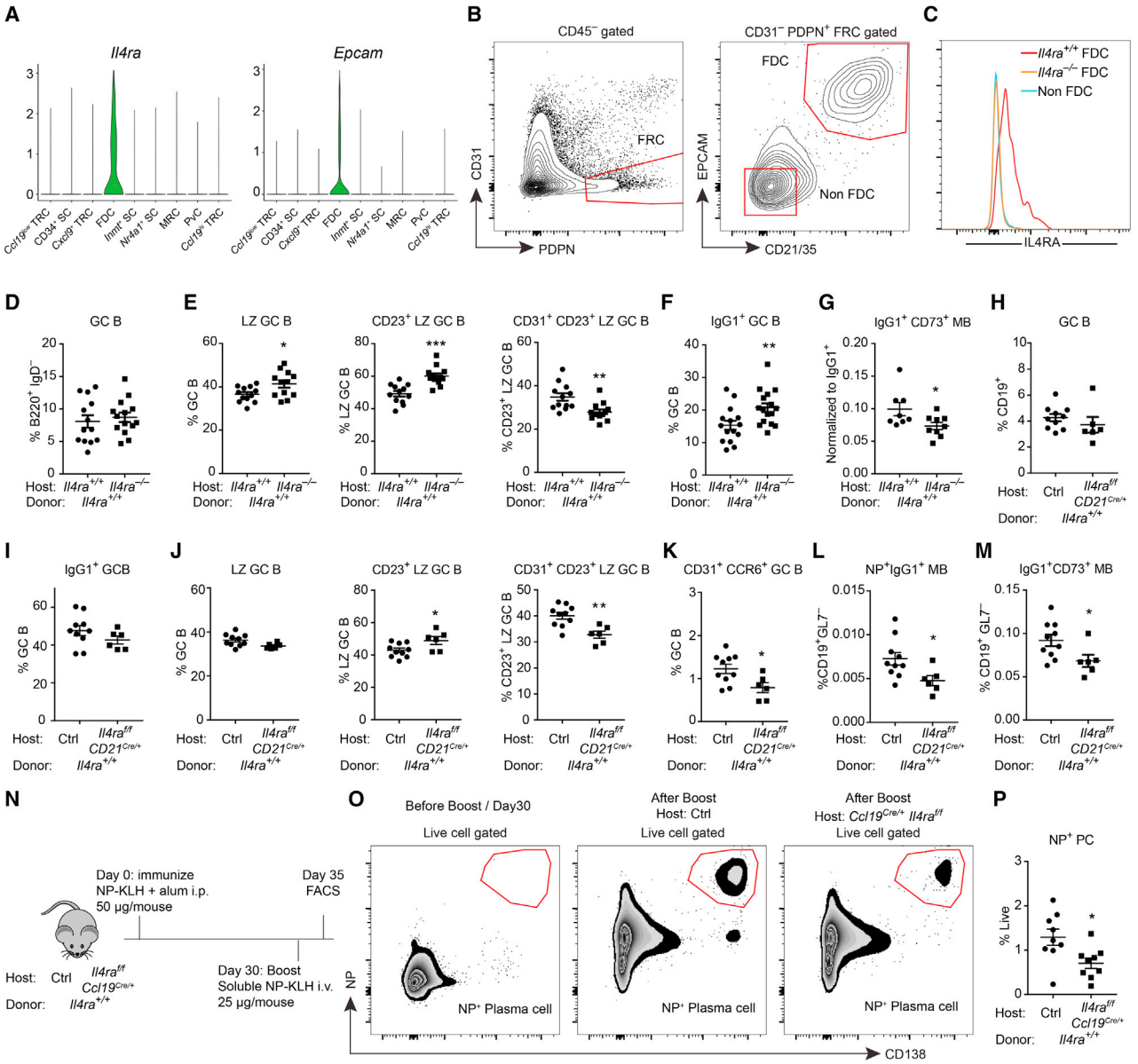

Figure 6. IL4RA expression by FDCs limits IL-4 availability to GC B cells

(A) Violin plots of *Il4ra* and *Epcam* expression in different stromal cell subsets.

(B and C) Representative FACS profiles (B) and histograms (C) of IL4RA in non-FDCs (CD45$^-$ PDPN$^+$ CD31$^-$ CD21/35$^-$ EPCAM$^-$) and FDCs (CD45$^-$ PDPN$^+$ CD31$^-$ CD21/35$^+$ EPCAM$^+$) isolated from mesenteric LNs in mice with indicated genotype. Data represent 2 experiments, with at least 3 mice per experiment.

(D–G) Reverse chimeras were made by reconstituting irradiated *Il4ra*$^{+/+}$ and *Il4ra*$^{-/-}$ mice with WT BM.

(D–F) Frequencies of CD95^{hi} GL7^{hi} GC B cells in B220$^+$ IgD$^-$ B cells (D), CXCR4^{lo} CD86^{hi} LZ cells in GC B cells (E, left), CD23$^+$ cells in LZ B cells (E, center), CD31$^+$ cells in CD23$^+$ LZ B cells (E, right), and IgG1$^+$ cells in GC B cells (F) 13 days after immunization.

(G) Ratio of CD73$^+$ IgG1$^+$ memory B cells to IgG1$^+$ cells. Data are pooled from 3 experiments.

(H–M) Reverse chimeras were made by reconstituting irradiated control and *CD21*$^{Cre/+}$ *Il4ra*$^{f/f}$ mice with wild-type (*Il4ra*$^{+/+}$) BM.

(H–K) Frequencies of CD95^{hi} GL7^{hi} GC B cells in CD19$^+$ B cells (H), IgG1$^+$ cells in GC B cells (I), LZ cells in GC B cells (J, left), CD23$^+$ cells in LZ B cells (J, center), CD31$^+$ cells in CD23$^+$ LZ B cells (J, right), and CD31$^+$ CCR6$^+$ cells in GC B cells (K) 13 days after immunization.

(L and M) Frequencies of NP$^+$IgG1$^+$ (L) and CD73$^+$ IgG1$^+$ (M) memory cells in non-GC B cells.

(N–P) Scheme for testing memory response in *Ccl19*$^{Cre/+}$ *Il4ra*$^{f/f}$ mice that had been reconstituted with wild-type BM (N), flow cytometry plots from the indicated mice (O), and summary data (P) showing frequency of CD138$^+$NP$^+$ plasma cells in the spleen of boosted control or *Ccl19*$^{Cre/+}$ *Il4ra*$^{f/f}$ chimeric mice.

Data are pooled from 2 of 3 experiments. In (D–M) and (P), each symbol represents 1 mouse. Data are presented as mean ± SEM; *$p < 0.05$, **$p < 0.01$, ***$p < 0.001$.

See also Figure S6.

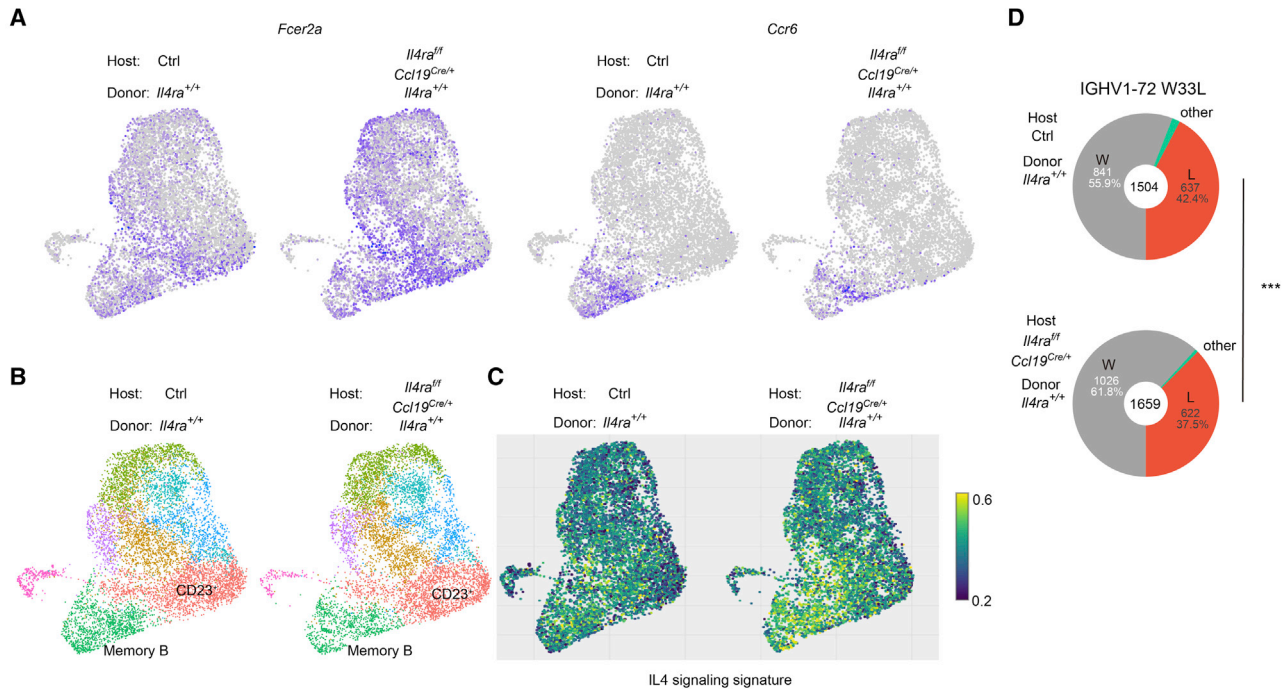

Figure 7. scRNA-seq analysis of stromal cell IL4Ra-deficient mice

(A–D) Reverse chimeras were made by reconstituting irradiated *Il4ra*$^{+/+}$ and *Ccl19*$^{Cre/+}$ *Il4ra*$^{f/f}$ mice with WT BM. scRNA-seq and scVDJ-seq was performed on B220^{+} CD95^{hi} GL7^{hi} IgD^{-} cells sorted at day 14 post-NP-KLH immunization. Cells from 4 mice were pooled together in each condition.

(A) UMAP plots of the expression of *Fcer2a* and *Ccr6*. Color scaled for each gene with log normalized expression level.

(B) UMAP plots of different clusters.

(C) Visualize signature scores of IL-4 signaling in GC B cells. Color scaled for signature score.

(D) Pie charts displaying the frequencies of W33L mutations in IGHV1-72*01 sequences. Chi-square test. ***$p < 0.001$.

See also Figure S7.

chimeras were boosted at 4 weeks and their plasma cell response was analyzed 5 days later. The stromal IL4Ra-deficient mice showed a significant reduction in the generation of secondary NP^{+} plasma cells compared to WT controls (Figures 6N–6P). These data are consistent with reduced memory cell generation when FDCs are unable to restrict IL-4 availability.

As a further approach to test for FDC IL4Ra-mediated restraint of IL-4 signaling in GC B cells, we performed scRNA-seq and scVDJ-seq on GC cells from WT and *Ccl19*$^{Cre/+}$ *Il4ra*$^{f/f}$ chimeras. Consistent with the flow cytometric findings, the expression of *Fcer2a* was increased and the expression of *Ccr6* was decreased in the GC B cells from stromal IL4Ra-deficient mice (Figure 7A). Clustering analysis also revealed a decrease in memory B cells (16.22% in WT and 12.92% in *Ccl19*$^{Cre/+}$ *Il4ra*$^{f/f}$) and plasma cells (3.58% in WT and 1.86% in *Ccl19*$^{Cre/+}$ *Il4ra*$^{f/f}$) (Figures 7B and S7A). We also calculated the signature score of IL-4 pathway activity by VISION, revealing an increase in IL-4 signaling in the stromal IL4Ra-deficient chimeras (Figure 7C).

Analysis of the scVDJ-seq data showed that there was no difference in the usage of IGHV1-72 heavy chain (Figure S7B) or in the class switch of IGHV1-72 (Figure S7C) between WT and *Ccl19*$^{Cre/+}$ *Il4ra*$^{f/f}$ chimeras. Importantly, however, there was a decrease in the frequency of W33L high-affinity cells in the *Ccl19*$^{Cre/+}$ *Il4ra*$^{f/f}$ chimeras (Figure 7D), suggesting a reduction in selection stringency when mice lack IL4Ra on FDCs. This was also suggested by a 30% enrichment for the affinity-reducing D50G mutation (Dal Porto et al., 1998) in the *Ccl19*$^{Cre/+}$ *Il4ra*$^{f/f}$ chimeras (0.937% in WT and 1.25% in *Ccl19*$^{Cre/+}$ *Il4ra*$^{f/f}$). Finally, we also used these data to further test the relationship between affinity and memory and again found that the frequency of W33L mutations was lower in the memory B cell than in the GC B cell and plasma cell compartments in both WT and *Ccl19*$^{Cre/+}$ *Il4ra*$^{f/f}$ chimeras (Figure S7D). Although Igλ^{+} cells are dominant in the NP GC response (Jack et al., 1977), their frequency in memory B cells was lower than in GC B cells and plasma cells (Figure S7E).

DISCUSSION

The experiments in this study were motivated by the finding from stromal cell scRNA-seq analysis that IL4Ra is expressed by FDCs (Rodda et al., 2018). Investigating the actions of IL-4 in the GC, we characterized an IL-4-responsive CD23^{+} LZ population of GC B cells that was enriched in pre-memory B cells and cells with features of pre-plasma cells. IL4Ra-STAT6 signaling was shown to disfavor pre-memory and memory cell development. Several lines of evidence indicated that IL-4 could act on bystander B cells within the GC. Using conditional gene-deficient mice, we found that FDC IL4Ra expression contributed to restraining IL-4 availability in the GC. We propose that FDC IL4Ra expression helps prevent non-cognate actions of IL-4 in the GC and thereby promotes antibody affinity maturation and

GC B cell differentiation. While IL-4 broadcasting by effector Th2 cells may be beneficial for type 2 immune responses, such as during worm expulsion, the non-cognate actions of IL-4 may be detrimental during selection events in GCs. We suggest that the GC evolved as a specialized microenvironment that enhances the ability of IL-4 to act in a targeted manner.

Our findings extend recent work establishing that scRNA-seq can be used to identify pre-memory and pre-plasma cells within the GC (Holmes et al., 2020; Laidlaw et al., 2020) and provide evidence that it can be used to identify cells at an even earlier stage that are projected to take on one or other of these fates. Signaling pathway network analysis (Chen et al., 2012) of the day 7 scRNA-seq data showed that the CD23$^+$ cluster was enriched for RelA activity (data not shown), in line with genetic studies showing that RelA was dispensable for GC maintenance but important for differentiation to post-GC states (Heise et al., 2014). The significance of the enriched BCR gene expression signature in the CD23$^+$ LZ cells is not yet clear, although some studies have suggested that BCR signaling is important for GC B cell differentiation into plasma cells (Kräutler et al., 2017; Li et al., 2018).

Recent reports have provided evidence that memory B cells are often of lower affinity than GC B cells that are sampled from the animal at the same time (Shinnakasu et al., 2016; Suan et al., 2017; Sundling et al., 2021), although this has not been seen in every case (Wang et al., 2017). A limitation in some of these studies has been the possibility that the memory B cells being sequenced were generated at an earlier stage in the response than the GC cells, a time when less affinity enhancing mutations had accrued. However, in some studies, the lower antigen binding ability was noted for pre-memory cells compared to contemporaneous GC cells (Shinnakasu et al., 2016; Suan et al., 2017). Our use of scVDJ-seq establishes a further approach to examine this issue and provides evidence supporting the conclusion that memory B cells and plasma cells are strongly selected for antigen binding, but cells taking on the memory fate are less strongly affinity matured than those taking on the plasma cell fate.

Cells expressing low levels of the plasma cell transcription factor Blimp1 have been identified among both LZ and DZ phenotype cells, with greater abundance in the DZ (Kräutler et al., 2017; Radtke and Bannard, 2019). Our RNA trajectory analysis suggests that some cells can take on early plasma cell gene expression properties while in a CD23$^+$ LZ state, including beginning to upregulate CXCR4, a key marker of the DZ state. These cells may therefore give rise to DZ pre-plasma cells. These observations do not exclude the possibility of pre-plasma cells also emerging separately through a pathway in the DZ. Moreover, even when cells reach a Blimp1-low state, their fate can be unstable, with some cells returning to a GC state (Radtke and Bannard, 2019).

CD23 expression by LZ cells has been previously noted, with expression being higher on pre-memory cells than most other GC cells, but the significance of this expression was not addressed (Gonzalez et al., 2018; Suan et al., 2017). The ability of IL-4 to cause induction of CD23$^+$ LZ cells, the detection of higher pStat6 in CD23$^+$ than CD23$^-$ LZ cells, and the evidence of IL-4 signaling pathway activity in the CD23$^+$ cell cluster provides evidence that CD23 marks IL-4-responding cells within the GC. CD23 can also be induced by CD40 signaling (Paterson et al., 1996; Siepmann et al., 1996), and we observed small numbers of cells in the Myc$^+$ cluster that had high *Fcer2a* transcript levels. The basis for their being a separate population of CD23^{hi} Myc$^{lo/-}$ cells is not yet clear, but they may reflect cells that have not yet received sufficient cognate T cell help to turn on Myc. We also suggest that some of the CD23$^+$ cells exhibiting IL-4 pathway activity in the absence of Myc expression may be cells receiving IL-4 in a bystander manner.

The role of IL-4 in GC responses has been examined in multiple studies, but with variable conclusions. The findings presented here agree with observations indicating that IL-4 is not universally required for mounting a GC response of normal magnitude. However, the data do add to evidence that IL-4 can augment the size of the LZ compartment (Gonzalez et al., 2018; Turqueti-Neves et al., 2014). We propose that IL-4 augments LZ cell accumulation at least in part by restraining effector cell output from the CD23$^+$ LZ compartment. IL-4 acts to intrinsically restrain CD23$^+$ LZ B cell differentiation into memory B cells. When IL4Ra is absent, the cells appear to transit more readily to a CD23$^+$CD31$^+$ pre-memory state, likely contributing to an overall reduction in the LZ and an enlargement of the memory compartment. We noted similar trends for IL4Ra in restraining plasma cell generation, and although this was less completely studied due to marker limitations, the finding is consistent with several *in vitro* studies (Ettinger et al., 2005; Jenks et al., 2018; Pignarre et al., 2021). Importantly, while it has been possible to track effects of IL-4 on memory cell output, we have not been able to assess to what extent CD23$^+$ LZ cells continue on to other stages of the GC. It is likely that some of the cells receive sufficient cumulative positive selection signals to undergo cyclic reentry to the DZ.

A key aspect of this study is the finding that FDC IL4Ra helps restrict IL-4 availability in the GC. Past work has highlighted that Tfh cells produce low amounts of IL-4 compared to Th2 cells, and this was suggested to be important for limiting IL-4 delivery to cognate partner B cells (Crotty, 2014). However, IL-4 was found to be broadcast from activated T cells *in vitro* and not released selectively at the synapse (Huse et al., 2006); and in accordance with this observation, our data indicate that when the IL4Ra abundance in GCs is reduced, non-cognate actions of IL-4 become notable. Moreover, our work adds support to the notion that the amounts of IL-4 acting in the GC need to be finely tuned since both too little and too much can be associated with LZ defects, less affinity maturation, and reduced GC responses; too much can also be associated with reduced memory and plasma cell generation. Our findings suggest that high IL4Ra expression on FDCs is part of the specialization of the GC microenvironment, helping establish a niche that limits non-cognate actions of IL-4. The mechanism of FDC IL4Ra action in restraining IL-4 availability is not yet clear, although IL4Ra has a well-established ability to mediate the internalization of IL-4 (Friedrich et al., 1999). It is also possible that soluble IL4Ra is generated, although whether this has positive or negative effects on IL-4 availability may be context dependent (Chilton and Fernandez-Botran, 1993; Khodoun et al., 2007). We speculate that in GCs containing some high-affinity B cells that trigger strong activation of Tfh cells, this leads to the transient production of sufficient amounts of IL-4 to overcome the depletion mechanisms of

the GC niche and promote the ongoing participation of bystander lower-affinity GC cells, helping sustain the diversity of individual GC responses.

Limitations of study

All of the experiments were performed with intraperitoneal immunizations and analysis of GC responses in the spleen. It is not yet known whether FDC IL4Ra will have equivalent functions in LNs or across other types of GC responses. A technical limitation was our inability to perform *ex vivo* pSTAT6 staining in stromal IL4Ra-deficient mice due to poor assay sensitivity. The lack of markers to track the emergence of pre-plasma cells was a limitation in assessing the accuracy of the trajectory analysis. We note that our study has not fully elucidated the effects of IL-4 signaling in GC B cells, such as determining target genes engaged by Stat6 or the fate of IL-4-stimulated cells that stay within the GC. Finally, we acknowledge that the clustering analysis has limitations in the precision with which it represents GC cells that are in a single state.

STAR★METHODS

Detailed methods are provided in the online version of this paper and include the following:

- KEY RESOURCES TABLE
- RESOURCE AVAILABILITY
  - Lead contact
  - Materials availability
  - Data and code availability
- EXPERIMENTAL MODEL AND SUBJECT DETAILS
  - Mice
- METHOD DETAILS
  - Immunization and treatment
  - Mixed or reverse bone marrow chimeras
  - Retroviral constructs and transductions
  - EdU labeling and analysis
  - IL4 injection and analysis
  - AS20-OVA stimulation
  - Flow cytometry
  - Immunofluorescent staining
  - Single cell sequencing and analysis
- QUANTIFICATION AND STATISTICAL ANALYSIS

SUPPLEMENTAL INFORMATION

Supplemental information can be found online at https://doi.org/10.1016/j.immuni.2021.08.028.

ACKNOWLEDGMENTS

We thank Chris Allen, Mark Ansel, Marlys Fassett, Rich Locksley, Burkhard Ludewig, and Takaharu Okada for the mice. This work was supported by grants from the NIH (R01AI045073). D.L. and H.C. were supported by the Irvington Cancer Research Institute. J.G.C. is an investigator of the Howard Hughes Medical Institute.

AUTHOR CONTRIBUTIONS

L.D., D.L., and J.G.C. designed the study; L.D. and D.L. performed the experiments; H.C. and M.A.M. generated cells for scRNA-seq and scVDJ-seq in Figures 1, 2, and 3; L.D. performed the scRNA-seq and scVDJ-seq analyses; H.C. and M.Y.C. characterized the AS20-OVA reagent; D.I.K. generated the pMCP-BFP vector; Y.X. generated AS20-OVA; J.A. screened the mice; B.J.L. provided input on the memory B cell characterization; L.D., D.L., and J.G.C. analyzed the data and wrote the manuscript.

DECLARATION OF INTERESTS

J.G.C. is an Scientific Advisory Board member of Be Biopharma and MiroBio.

Received: April 19, 2020
Revised: June 2, 2021
Accepted: August 27, 2021
Published: September 22, 2021

REFERENCES

Anderson, S.M., Tomayko, M.M., Ahuja, A., Haberman, A.M., and Shlomchik, M.J. (2007). New markers for murine memory B cells that define mutated and unmutated subsets. J. Exp. Med. *204*, 2103–2114.

Andoh, A., Masuda, A., Yamakawa, M., Kumazawa, Y., and Kasajima, T. (2000). Absence of interleukin-4 enhances germinal center reaction in secondary immune response. Immunol. Lett. *73*, 35–41.

Bannard, O., and Cyster, J.G. (2017). Germinal centers: programmed for affinity maturation and antibody diversification. Curr. Opin. Immunol. *45*, 21–30.

Bemark, M., Hazanov, H., Strömberg, A., Komban, R., Holmqvist, J., Köster, S., Mattsson, J., Sikora, P., Mehr, R., and Lycke, N.Y. (2016). Limited clonal relatedness between gut IgA plasma cells and memory B cells after oral immunization. Nat. Commun. *7*, 12698.

Bergen, V., Lange, M., Peidli, S., Wolf, A., and Theis, F.J. (2020). Generalizing RNA velocity to transient cell states through dynamical modeling. bioRxiv. https://doi.org/10.1101/820936.

Boscardin, S.B., Hafalla, J.C., Masilamani, R.F., Kamphorst, A.O., Zebroski, H.A., Rai, U., Morrot, A., Zavala, F., Steinman, R.M., Nussenzweig, R.S., and Nussenzweig, M.C. (2006). Antigen targeting to dendritic cells elicits long-lived T cell help for antibody responses. J. Exp. Med. *203*, 599–606.

Calado, D.P., Sasaki, Y., Godinho, S.A., Pellerin, A., Köchert, K., Sleckman, B.P., de Alborán, I.M., Janz, M., Rodig, S., and Rajewsky, K. (2012). The cell-cycle regulator c-Myc is essential for the formation and maintenance of germinal centers. Nat. Immunol. *13*, 1092–1100.

Chai, Q., Onder, L., Scandella, E., Gil-Cruz, C., Perez-Shibayama, C., Cupovic, J., Danuser, R., Sparwasser, T., Luther, S.A., Thiel, V., et al. (2013). Maturation of lymph node fibroblastic reticular cells from myofibroblastic precursors is critical for antiviral immunity. Immunity *38*, 1013–1024.

Chen, E.Y., Xu, H., Gordonov, S., Lim, M.P., Perkins, M.H., and Ma'ayan, A. (2012). Expression2Kinases: mRNA profiling linked to multiple upstream regulatory layers. Bioinformatics *28*, 105–111.

Cheng, H.W., Onder, L., Novkovic, M., Soneson, C., Lütge, M., Pikor, N., Scandella, E., Robinson, M.D., Miyazaki, J.I., Tersteegen, A., et al. (2019). Origin and differentiation trajectories of fibroblastic reticular cells in the splenic white pulp. Nat. Commun. *10*, 1739.

Chevrier, S., Kratina, T., Emslie, D., Tarlinton, D.M., and Corcoran, L.M. (2017). IL4 and IL21 cooperate to induce the high Bcl6 protein level required for germinal center formation. Immunol. Cell Biol. *95*, 925–932.

Chilton, P.M., and Fernandez-Botran, R. (1993). Production of soluble IL-4 receptors by murine spleen cells is regulated by T cell activation and IL-4. J. Immunol. *151*, 5907–5917.

Cortes-Selva, D., Ready, A., Gibbs, L., Rajwa, B., and Fairfax, K.C. (2019). IL-4 promotes stromal cell expansion and is critical for development of a type-2, but not a type 1 immune response. Eur. J. Immunol. *49*, 428–442.

Crooks, G.E., Hon, G., Chandonia, J.M., and Brenner, S.E. (2004). WebLogo: a sequence logo generator. Genome Res. *14*, 1188–1190.

Crotty, S. (2014). T follicular helper cell differentiation, function, and roles in disease. Immunity *41*, 529–542.

Cunningham, A.F., Serre, K., Toellner, K.M., Khan, M., Alexander, J., Brombacher, F., and MacLennan, I.C.M. (2004). Pinpointing IL-4-independent

acquisition and IL-4-influenced maintenance of Th2 activity by CD4 T cells. Eur. J. Immunol. *34*, 686–694.

Dal Porto, J.M., Haberman, A.M., Shlomchik, M.J., and Kelsoe, G. (1998). Antigen drives very low affinity B cells to become plasmacytes and enter germinal centers. J. Immunol. *161*, 5373–5381.

Defrance, T., Aubry, J.P., Rousset, F., Vanbervliet, B., Bonnefoy, J.Y., Arai, N., Takebe, Y., Yokota, T., Lee, F., Arai, K., et al. (1987). Human recombinant interleukin 4 induces Fc epsilon receptors (CD23) on normal human B lymphocytes. J. Exp. Med. *165*, 1459–1467.

DeTomaso, D., Jones, M.G., Subramaniam, M., Ashuach, T., Ye, C.J., and Yosef, N. (2019). Functional interpretation of single cell similarity maps. Nat. Commun. *10*, 4376.

Dominguez-Sola, D., Victora, G.D., Ying, C.Y., Phan, R.T., Saito, M., Nussenzweig, M.C., and Dalla-Favera, R. (2012). The proto-oncogene MYC is required for selection in the germinal center and cyclic reentry. Nat. Immunol. *13*, 1083–1091.

Dubey, L.K., Karempudi, P., Luther, S.A., Ludewig, B., and Harris, N.L. (2017). Interactions between fibroblastic reticular cells and B cells promote mesenteric lymph node lymphangiogenesis. Nat. Commun. *8*, 367.

Ersching, J., Efeyan, A., Mesin, L., Jacobsen, J.T., Pasqual, G., Grabiner, B.C., Dominguez-Sola, D., Sabatini, D.M., and Victora, G.D. (2017). Germinal Center Selection and Affinity Maturation Require Dynamic Regulation of mTORC1 Kinase. Immunity *46*, 1045–1058.e6.

Ettinger, R., Sims, G.P., Fairhurst, A.M., Robbins, R., da Silva, Y.S., Spolski, R., Leonard, W.J., and Lipsky, P.E. (2005). IL-21 induces differentiation of human naive and memory B cells into antibody-secreting plasma cells. J. Immunol. *175*, 7867–7879.

Finkelman, F.D., Madden, K.B., Morris, S.C., Holmes, J.M., Boiani, N., Katona, I.M., and Maliszewski, C.R. (1993). Anti-cytokine antibodies as carrier proteins. Prolongation of in vivo effects of exogenous cytokines by injection of cytokine-anti-cytokine antibody complexes. J. Immunol. *151*, 1235–1244.

Finkin, S., Hartweger, H., Oliveira, T.Y., Kara, E.E., and Nussenzweig, M.C. (2019). Protein Amounts of the MYC Transcription Factor Determine Germinal Center B Cell Division Capacity. Immunity *51*, 324–336.e5.

Friedrich, K., Kammer, W., Erhardt, I., Brändlein, S., Arnold, S., and Sebald, W. (1999). The two subunits of the interleukin-4 receptor mediate independent and distinct patterns of ligand endocytosis. Eur. J. Biochem. *265*, 457–465.

Fu, Y.-X., and Chaplin, D.D. (1999). Development and maturation of secondary lymphoid tissues. Annu. Rev. Immunol. *17*, 399–433.

Gaya, M., Barral, P., Burbage, M., Aggarwal, S., Montaner, B., Warren Navia, A., Aid, M., Tsui, C., Maldonado, P., Nair, U., et al. (2018). Initiation of Antiviral B Cell Immunity Relies on Innate Signals from Spatially Positioned NKT Cells. Cell *172*, 517–533.e20.

Gitlin, A.D., von Boehmer, L., Gazumyan, A., Shulman, Z., Oliveira, T.Y., and Nussenzweig, M.C. (2016). Independent Roles of Switching and Hypermutation in the Development and Persistence of B Lymphocyte Memory. Immunity *44*, 769–781.

Gonzalez, D.G., Cote, C.M., Patel, J.R., Smith, C.B., Zhang, Y., Nickerson, K.M., Zhang, T., Kerfoot, S.M., and Haberman, A.M. (2018). Nonredundant Roles of IL-21 and IL-4 in the Phased Initiation of Germinal Center B Cells and Subsequent Self-Renewal Transitions. J. Immunol. *201*, 3569–3579.

Granato, A., Hayashi, E.A., Baptista, B.J., Bellio, M., and Nobrega, A. (2014). IL-4 regulates Bim expression and promotes B cell maturation in synergy with BAFF conferring resistance to cell death at negative selection checkpoints. J. Immunol. *192*, 5761–5775.

Haberman, A.M., Gonzalez, D.G., Wong, P., Zhang, T.T., and Kerfoot, S.M. (2019). Germinal center B cell initiation, GC maturation, and the coevolution of its stromal cell niches. Immunol. Rev. *288*, 10–27.

Haniuda, K., Fukao, S., and Kitamura, D. (2020). Metabolic Reprogramming Induces Germinal Center B Cell Differentiation through Bcl6 Locus Remodeling. Cell Rep. *33*, 108333.

He, J.S., Subramaniam, S., Narang, V., Srinivasan, K., Saunders, S.P., Carbajo, D., Wen-Shan, T., Hidayah Hamadee, N., Lum, J., Lee, A., et al. (2017). IgG1 memory B cells keep the memory of IgE responses. Nat. Commun. *8*, 641.

Heise, N., De Silva, N.S., Silva, K., Carette, A., Simonetti, G., Pasparakis, M., and Klein, U. (2014). Germinal center B cell maintenance and differentiation are controlled by distinct NF-κB transcription factor subunits. J. Exp. Med. *211*, 2103–2118.

Herbert, D.R., Hölscher, C., Mohrs, M., Arendse, B., Schwegmann, A., Radwanska, M., Leeto, M., Kirsch, R., Hall, P., Mossmann, H., et al. (2004). Alternative macrophage activation is essential for survival during schistosomiasis and downmodulates T helper 1 responses and immunopathology. Immunity *20*, 623–635.

Holmes, A.B., Corinaldesi, C., Shen, Q., Kumar, R., Compagno, N., Wang, Z., Nitzan, M., Grunstein, E., Pasqualucci, L., Dalla-Favera, R., and Basso, K. (2020). Single-cell analysis of germinal-center B cells informs on lymphoma cell of origin and outcome. J. Exp. Med. *217*, e20200483.

Huse, M., Lillemeier, B.F., Kuhns, M.S., Chen, D.S., and Davis, M.M. (2006). T cells use two directionally distinct pathways for cytokine secretion. Nat. Immunol. *7*, 247–255.

Ise, W., Fujii, K., Shiroguchi, K., Ito, A., Kometani, K., Takeda, K., Kawakami, E., Yamashita, K., Suzuki, K., Okada, T., and Kurosaki, T. (2018). T Follicular Helper Cell-Germinal Center B Cell Interaction Strength Regulates Entry into Plasma Cell or Recycling Germinal Center Cell Fate. Immunity *48*, 702–715.e4.

Jack, R.S., Imanishi-Kari, T., and Rajewsky, K. (1977). Idiotypic analysis of the response of C57BL/6 mice to the (4-hydroxy-3-nitrophenyl)acetyl group. Eur. J. Immunol. *7*, 559–565.

Jacob, J., Przylepa, J., Miller, C., and Kelsoe, G. (1993). In situ studies of the primary immune response to (4-hydroxy-3-nitrophenyl)acetyl. III. The kinetics of V region mutation and selection in germinal center B cells. J. Exp. Med. *178*, 1293–1307.

Jelinek, D.F., and Lipsky, P.E. (1988). Inhibitory influence of IL-4 on human B cell responsiveness. J. Immunol. *141*, 164–173.

Jenks, S.A., Cashman, K.S., Zumaquero, E., Marigorta, U.M., Patel, A.V., Wang, X., Tomar, D., Woodruff, M.C., Simon, Z., Bugrovsky, R., et al. (2018). Distinct Effector B Cells Induced by Unregulated Toll-like Receptor 7 Contribute to Pathogenic Responses in Systemic Lupus Erythematosus. Immunity *49*, 725–739.e6.

Kaji, T., Ishige, A., Hikida, M., Taka, J., Hijikata, A., Kubo, M., Nagashima, T., Takahashi, Y., Kurosaki, T., Okada, M., et al. (2012). Distinct cellular pathways select germline-encoded and somatically mutated antibodies into immunological memory. J. Exp. Med. *209*, 2079–2097.

Kallies, A., Hasbold, J., Tarlinton, D.M., Dietrich, W., Corcoran, L.M., Hodgkin, P.D., and Nutt, S.L. (2004). Plasma cell ontogeny defined by quantitative changes in blimp-1 expression. J. Exp. Med. *200*, 967–977.

Khodoun, M., Lewis, C.C., Yang, J.Q., Orekov, T., Potter, C., Wynn, T., Mentink-Kane, M., Hershey, G.K., Wills-Karp, M., and Finkelman, F.D. (2007). Differences in expression, affinity, and function of soluble (s)IL-4Ralpha and sIL-13Ralpha2 suggest opposite effects on allergic responses. J. Immunol. *179*, 6429–6438.

Kotov, D.I., Mitchell, J.S., Pengo, T., Ruedl, C., Way, S.S., Langlois, R.A., Fife, B.T., and Jenkins, M.K. (2019). TCR Affinity Biases Th Cell Differentiation by Regulating CD25, Eef1e1, and Gbp2. J. Immunol. *202*, 2535–2545.

Kowalczyk, M.S., Tirosh, I., Heckl, D., Rao, T.N., Dixit, A., Haas, B.J., Schneider, R.K., Wagers, A.J., Ebert, B.L., and Regev, A. (2015). Single-cell RNA-seq reveals changes in cell cycle and differentiation programs upon aging of hematopoietic stem cells. Genome Res. *25*, 1860–1872.

Kraus, M., Alimzhanov, M.B., Rajewsky, N., and Rajewsky, K. (2004). Survival of resting mature B lymphocytes depends on BCR signaling via the Igalpha/beta heterodimer. Cell *117*, 787–800.

Kräutler, N.J., Suan, D., Butt, D., Bourne, K., Hermes, J.R., Chan, T.D., Sundling, C., Kaplan, W., Schofield, P., Jackson, J., et al. (2017). Differentiation of germinal center B cells into plasma cells is initiated by high-affinity antigen and completed by Tfh cells. J. Exp. Med. *214*, 1259–1267.

La Manno, G., Soldatov, R., Zeisel, A., Braun, E., Hochgerner, H., Petukhov, V., Lidschreiber, K., Kastriti, M.E., Lönnerberg, P., Furlan, A., et al. (2018). RNA velocity of single cells. Nature *560*, 494–498.

Laidlaw, B.J., Duan, L., Xu, Y., Vazquez, S.E., and Cyster, J.G. (2020). The transcription factor Hhex cooperates with the corepressor Tle3 to promote memory B cell development. Nat. Immunol. *21*, 1082–1093.

Laidlaw, B.J., Schmidt, T.H., Green, J.A., Allen, C.D., Okada, T., and Cyster, J.G. (2017). The Eph-related tyrosine kinase ligand Ephrin-B1 marks germinal center and memory precursor B cells. J. Exp. Med. *214*, 639–649.

Li, X., Gadzinsky, A., Gong, L., Tong, H., Calderon, V., Li, Y., Kitamura, D., Klein, U., Langdon, W.Y., Hou, F., et al. (2018). Cbl Ubiquitin Ligases Control B Cell Exit from the Germinal-Center Reaction. Immunity *48*, 530–541.e6.

Luther, S.A., Bidgol, A., Hargreaves, D.C., Schmidt, A., Xu, Y., Paniyadi, J., Matloubian, M., and Cyster, J.G. (2002). Differing activities of homeostatic chemokines CCL19, CCL21, and CXCL12 in lymphocyte and dendritic cell recruitment and lymphoid neogenesis. J. Immunol. *169*, 424–433.

Mackay, F., and Browning, J.L. (1998). Turning off follicular dendritic cells. Nature *395*, 26–27.

MacLennan, I.C.M. (1994). Germinal centers. Annu. Rev. Immunol. *12*, 117–139.

McCormick, S.M., and Heller, N.M. (2015). Commentary: IL-4 and IL-13 receptors and signaling. Cytokine *75*, 38–50.

Milpied, P., Cervera-Marzal, I., Mollichella, M.L., Tesson, B., Brisou, G., Traverse-Glehen, A., Salles, G., Spinelli, L., and Nadel, B. (2018). Human germinal center transcriptional programs are de-synchronized in B cell lymphoma. Nat. Immunol. *19*, 1013–1024.

Mokada-Gopal, L., Boeser, A., Lehmann, C.H.K., Drepper, F., Dudziak, D., Warscheid, B., and Voehringer, D. (2017). Identification of Novel STAT6-Regulated Proteins in Mouse B Cells by Comparative Transcriptome and Proteome Analysis. J. Immunol. *198*, 3737–3745.

Moriyama, S., Takahashi, N., Green, J.A., Hori, S., Kubo, M., Cyster, J.G., and Okada, T. (2014). Sphingosine-1-phosphate receptor 2 is critical for follicular helper T cell retention in germinal centers. J. Exp. Med. *211*, 1297–1305.

Muramatsu, M., Kinoshita, K., Fagarasan, S., Yamada, S., Shinkai, Y., and Honjo, T. (2000). Class switch recombination and hypermutation require activation-induced cytidine deaminase (AID), a potential RNA editing enzyme. Cell *102*, 553–563.

Onodera, T., Takahashi, Y., Yokoi, Y., Ato, M., Kodama, Y., Hachimura, S., Kurosaki, T., and Kobayashi, K. (2012). Memory B cells in the lung participate in protective humoral immune responses to pulmonary influenza virus reinfection. Proc. Natl. Acad. Sci. USA *109*, 2485–2490.

Paterson, R.L., Lack, G., Domenico, J.M., Delespesse, G., Leung, D.Y., Finkel, T.H., and Gelfand, E.W. (1996). Triggering through CD40 promotes interleukin-4-induced CD23 production and enhanced soluble CD23 release in atopic disease. Eur. J. Immunol. *26*, 1979–1984.

Perona-Wright, G., Mohrs, K., and Mohrs, M. (2010). Sustained signaling by canonical helper T cell cytokines throughout the reactive lymph node. Nat. Immunol. *11*, 520–526.

Pignarre, A., Chatonnet, F., Caron, G., Haas, M., Desmots, F., and Fest, T. (2021). Plasmablasts derive from CD23- activated B cells after the extinction of IL-4/STAT6 signaling and IRF4 induction. Blood *137*, 1166–1180.

Qiu, X., Hill, A., Packer, J., Lin, D., Ma, Y.A., and Trapnell, C. (2017). Single-cell mRNA quantification and differential analysis with Census. Nat. Methods *14*, 309–315.

Radtke, D., and Bannard, O. (2019). Expression of the Plasma Cell Transcriptional Regulator Blimp-1 by Dark Zone Germinal Center B Cells During Periods of Proliferation. Front. Immunol. *9*, 3106.

Reinhardt, R.L., Liang, H.E., and Locksley, R.M. (2009). Cytokine-secreting follicular T cells shape the antibody repertoire. Nat. Immunol. *10*, 385–393.

Reiter, R., and Pfeffer, K. (2002). Impaired germinal centre formation and humoral immune response in the absence of CD28 and interleukin-4. Immunology *106*, 222–228.

Ricardo-Gonzalez, R.R., Red Eagle, A., Odegaard, J.I., Jouihan, H., Morel, C.R., Heredia, J.E., Mukundan, L., Wu, D., Locksley, R.M., and Chawla, A. (2010). IL-4/STAT6 immune axis regulates peripheral nutrient metabolism and insulin sensitivity. Proc. Natl. Acad. Sci. USA *107*, 22617–22622.

Robinson, M.J., Pitt, C., Brodie, E.J., Valk, A.M., O'Donnell, K., Nitschke, L., Jones, S., and Tarlinton, D.M. (2019). BAFF, IL-4 and IL-21 separably program germinal center-like phenotype acquisition, BCL6 expression, proliferation and survival of CD40L-activated B cells in vitro. Immunol. Cell Biol. *97*, 826–839.

Roco, J.A., Mesin, L., Binder, S.C., Nefzger, C., Gonzalez-Figueroa, P., Canete, P.F., Ellyard, J., Shen, Q., Robert, P.A., Cappello, J., et al. (2019). Class-Switch Recombination Occurs Infrequently in Germinal Centers. Immunity *51*, 337–350.e7.

Rodda, L.B., Lu, E., Bennett, M.L., Sokol, C.L., Wang, X., Luther, S.A., Barres, B.A., Luster, A.D., Ye, C.J., and Cyster, J.G. (2018). Single-Cell RNA Sequencing of Lymph Node Stromal Cells Reveals Niche-Associated Heterogeneity. Immunity *48*, 1014–1028.e6.

Schwickert, T.A., Alabyev, B., Manser, T., and Nussenzweig, M.C. (2009). Germinal center reutilization by newly activated B cells. J. Exp. Med. *206*, 2907–2914.

Shinnakasu, R., Inoue, T., Kometani, K., Moriyama, S., Adachi, Y., Nakayama, M., Takahashi, Y., Fukuyama, H., Okada, T., and Kurosaki, T. (2016). Regulated selection of germinal-center cells into the memory B cell compartment. Nat. Immunol. *17*, 861–869.

Siepmann, K., Wohlleben, G., and Gray, D. (1996). CD40-mediated regulation of interleukin-4 signaling pathways in B lymphocytes. Eur. J. Immunol. *26*, 1544–1552.

Suan, D., Kräutler, N.J., Maag, J.L.V., Butt, D., Bourne, K., Hermes, J.R., Avery, D.T., Young, C., Statham, A., Elliott, M., et al. (2017). CCR6 Defines Memory B Cell Precursors in Mouse and Human Germinal Centers, Revealing Light-Zone Location and Predominant Low Antigen Affinity. Immunity *47*, 1142–1153.e4.

Sundling, C., Lau, A.W.Y., Bourne, K., Young, C., Laurianto, C., Hermes, J.R., Menzies, R.J., Butt, D., Kräutler, N.J., Zahra, D., et al. (2021). Positive selection of IgG^+ over IgM^+ B cells in the germinal center reaction. Immunity *54*, 988–1001.e5.

Takeda, K., Tanaka, T., Shi, W., Matsumoto, M., Minami, M., Kashiwamura, S., Nakanishi, K., Yoshida, N., Kishimoto, T., and Akira, S. (1996). Essential role of Stat6 in IL-4 signalling. Nature *380*, 627–630.

Taylor, J.J., Pape, K.A., and Jenkins, M.K. (2012). A germinal center-independent pathway generates unswitched memory B cells early in the primary response. J. Exp. Med. *209*, 597–606.

Tomayko, M.M., Steinel, N.C., Anderson, S.M., and Shlomchik, M.J. (2010). Cutting edge: hierarchy of maturity of murine memory B cell subsets. J. Immunol. *185*, 7146–7150.

Turqueti-Neves, A., Otte, M., Prazeres da Costa, O., Höpken, U.E., Lipp, M., Buch, T., and Voehringer, D. (2014). B-cell-intrinsic STAT6 signaling controls germinal center formation. Eur. J. Immunol. *44*, 2130–2138.

Vajdy, M., Kosco-Vilbois, M.H., Kopf, M., Köhler, G., and Lycke, N. (1995). Impaired mucosal immune responses in interleukin 4-targeted mice. J. Exp. Med. *181*, 41–53.

Viant, C., Weymar, G.H.J., Escolano, A., Chen, S., Hartweger, H., Cipolla, M., Gazumyan, A., and Nussenzweig, M.C. (2020). Antibody Affinity Shapes the Choice between Memory and Germinal Center B Cell Fates. Cell *183*, 1298–1311.e11.

Victora, G.D., Dominguez-Sola, D., Holmes, A.B., Deroubaix, S., Dalla-Favera, R., and Nussenzweig, M.C. (2012). Identification of human germinal center light and dark zone cells and their relationship to human B-cell lymphomas. Blood *120*, 2240–2248.

Victora, G.D., and Nussenzweig, M.C. (2012). Germinal centers. Annu. Rev. Immunol. *30*, 429–457.

Victora, G.D., Schwickert, T.A., Fooksman, D.R., Kamphorst, A.O., Meyer-Hermann, M., Dustin, M.L., and Nussenzweig, M.C. (2010). Germinal center dynamics revealed by multiphoton microscopy with a photoactivatable fluorescent reporter. Cell *143*, 592–605.

Wang, X., Rodda, L.B., Bannard, O., and Cyster, J.G. (2014). Integrin-mediated interactions between B cells and follicular dendritic cells influence germinal center B cell fitness. J. Immunol. *192*, 4601–4609.

Wang, Y., Shi, J., Yan, J., Xiao, Z., Hou, X., Lu, P., Hou, S., Mao, T., Liu, W., Ma, Y., et al. (2017). Germinal-center development of memory B cells driven by IL-9 from follicular helper T cells. Nat. Immunol. *18*, 921–930.

Wills-Karp, M., and Finkelman, F.D. (2008). Untangling the complex web of IL-4- and IL-13-mediated signaling pathways. Sci. Signal. *1*, pe55.

Zhang, Y., Tech, L., George, L.A., Acs, A., Durrett, R.E., Hess, H., Walker, L.S.K., Tarlinton, D.M., Fletcher, A.L., Hauser, A.E., and Toellner, K.M. (2018). Plasma cell output from germinal centers is regulated by signals from Tfh and stromal cells. J. Exp. Med. *215*, 1227–1243.

STAR★METHODS

KEY RESOURCES TABLE

REAGENT or RESOURCE	SOURCE	IDENTIFIER
Antibodies		
anti-CD19 BV785 (clone 1D3)	BD Bioscience	Cat#563333; RRID: AB_2738141
anti-B220 BV785 (clone RA3-6B2)	BioLegend	Cat#103246; RRID: AB_2563256
anti-IgD FITC (clone 11-26c.2a)	BioLegend	Cat#405704; RRID: AB_394859
anti-IgD Alexa Fluor 647 (clone 11-26c.2a)	BioLegend	Cat#405708; RRID: AB_893528
anti-IgD Pacific Blue (clone 11-26c.2a)	BioLegend	Cat#405712; RRID: AB_1937244
anti-IgD BV605	BD Bioscience	Cat#563003; RRID: AB_2737944
anti-IgD PerCP/Cy5.5	BioLegend	Cat#405710; RRID: AB_1575113
anti-GL-7 (Ly-77) Pacific Blue (clone GL7)	BioLegend	Cat#144614; RRID: AB_2563292
anti-GL-7 (Ly-77) FITC (clone GL7)	BioLegend	Cat#144604; RRID: AB_2561697
anti-CD95 PE-CY7 (clone Jo2)	BD Bioscience	Cat#557653; RRID: AB_396768
anti-CD45.1 PERCP-CY5.5 (clone A20)	Tonbo	Cat#65-0453-U100
anti-CD45.1 BV605 (clone A20)	BioLegend	Cat#110738; RRID: AB_2562565
anti-CD45.2 BV605 (clone 104)	BioLegend	Cat#109841; RRID: AB_2563485
anti-Ephrin-B1 Biotin (polyclonal)	R&D	Cat#BAF473; RRID: AB_2293418
anti-CXCR4 Biotin (clone 2B11)	BD Bioscience	Cat#551968; RRID: AB_394307
anti-CD86 BV605	Biolegend	Cat#105037; RRID: AB_11204429
anti-IgG1 FITC (clone RMG1-1)	BioLegend	Cat#406606; RRID: AB_493293
anti-IgG1 APC	BioLegend	Cat#406610; RRID: AB_10696420
anti-CD138 BV421 (clone 281-2)	BioLegend	Cat#142508; RRID: AB_11203544
anti-CD138 BV711 (clone 281-2)	BD Bioscience	Cat#563193; RRID: AB_2631190
anti-CD98 BV711	BD Bioscience	Cat#745466; RRID: AB_2743009
anti-CD73 PERCP-CY5.5 (clone TY/11.8)	BioLegend	Cat#127214; RRID: AB_11219403
anti-gp38 APC (clone 8.1.1)	BioLegend	Cat#127410; RRID: AB_10613649
anti-CD31 PE (clone MEC 13.3)	BD Biosciences	Cat#553373; RRID: AB_394819
anti-CD31 PE-Cy7 (clone MEC 13.3)	BioLegend	Cat#102417; RRID: AB_830756
anti-Epcam BV711	BioLegend	Cat#118233; RRID: AB_2632775
anti-CD21/35 pacific Blue	BioLegend	Cat#123414; RRID: AB_2085158
Streptavidin BV711	BD Bioscience	Cat#563262; RRID: AB_2869478
anti-CD79b FITC	BD Bioscience	Cat#555303; RRID: AB_395717
anti-CD23 Alexa Fluor 488	BioLegend	Cat#101609; RRID: AB_493362
anti-CD23 Alexa Fluor 647	BioLegend	Cat#101612; RRID: AB_2103038
anti-CD72	BD Bioscience	Cat#550268; RRID: AB_393565
anti-IL4ra PE (Clone mIL4R-M1)	BD Bioscience	Cat#552509; RRID: AB_394407
anti-IL4 (clone 11B11)	Bio X cell	Cat#BE0045; RRID: AB_1107707
Fixable Viability Dye eFluor780	eBioscience	Cat#65-0865-14
anti-CD38 PE-Cy7	BioLegend	Cat#102718; RRID: AB_2275531
anti-CD38 FITC	BioLegend	Cat# 102705; RRID: AB_312926
anti-CD196 Alexa Fluor 647	BD Bioscience	Cat#557976; RRID: AB_2228793
anti-Ki67 Alexa Fluor 647	BD Bioscience	Cat#558615; RRID: AB_647130
anti-Bcl-6 Alexa Fluor 647	BD Bioscience	Cat#561525; RRID: AB_10898007
anti-pStat6 (Tyr641) (46H1L12)	Thermo Fisher Scientific	Cat# 700247; RRID: AB_2532305
Cy3 AffiniPure Goat Anti-Rabbit	Jackson ImmunoResearch	Cat#111-165-144; RRID: AB_2338006
Rabbit anti-Tmem119	B. Barres	Rodda et al., 2018

(*Continued on next page*)

Continued

REAGENT or RESOURCE	SOURCE	IDENTIFIER
AS20/anti-CD45.1 -OVA	This paper	N/A
Chemicals, peptides, and recombinant proteins		
Lipopolysaccharides (*Escherichia coli*, serotype O111:B4)	Sigma	Cat# L2630-25MG
NP-CGG	Biosearch Technologies	Cat#N-5055C-5
NP-KLH	Biosearch Technologies	Cat#N-5060
NP-PE	Biosearch Technologies	Cat#N-5070-1
Collagenase IV	Worthington Biochemical	Cat#LS004188
DNase I, bovine pancreas (single cell stromal cell analysis)	Sigma-Aldrich	Cat#DN25
EdU (5-ethynyl-2′-deoxyuridine)	Setareh Biotech	Cat#7180
mLTbR-huIgG1 (LTbR-Fc)	J. Browning	N/A
Aluminum hydroxide gel	Invivogen	Cat#vac-alu-250
Murine recombinant IL-4	PeproTech	Cat#214-14
Critical commercial assays		
Chromium Single Cell 5′ Library & Gel Bead Kit	10x Genomics	Cat#1000014
Chromium i7 Multiplex Kit	10x Genomics	Cat#120262
Chromium Single Cell A Chip Kit	10x Genomics	Cat#1000151
Chromium Single Cell 5′ Library Construction Kit	10x Genomics	Cat#1000020
Chromium Single Cell V(D)J Enrichment Kit, Mouse B Cell	10x Genomics	Cat#1000072
Click-iT Plus EdU Alexa Fluor 647 Flow Cytometry Assay Kit 100 Tests	Invitrogen	Cat#C10635
Lipofectamine 2000 Transfection Reagent	Thermo Fisher Scientific	Cat# 11668500
Deposited data		
10x single cell RNA-seq data	This paper	GSE180920
BCR heavy chain sequencing data	This paper	Table S4
IL4 incubation RNA-seq data	Mokada-Gopal et al., 2017	GSE84075
Spleen stromal cell single cell RNA-seq data	Cheng et al., 2019	E-MTAB-7703, E-MTAB-7094
NP-specific high- and low-affinity GC B cell RNA-seq data	Shinnakasu et al., 2016	GSE73729
Pre plasma cell RNA-seq data	Ise et al., 2018	GSE109732
Post GC B cell RNA-seq data	Laidlaw et al., 2017	GSE89897
Pre memory B cell RNA-seq data	Wang et al., 2017	GSE85018
Experimental models: cell lines		
Platinum-E (Plat-E) Retroviral Packaging Cell Line	Gift from S. Schwab	N/A
Experimental models: organisms/strains		
Mouse: C57BL/6J	The Jackson Laboratory	JAX: 000664
Mouse: B6.SJL-*Ptprc*^{a} *Pepc*^{b}/BoyJ	The Jackson Laboratory	JAX: 002014
Mouse: Rosa26-LSL-Cas9	The Jackson Laboratory	JAX: 024857
Mouse: *Il4ra*$^{-/-}$	The Jackson Laboratory	JAX:003514
Mouse: *Cγ1*$^{Cre/+}$	The Jackson Laboratory	JAX: 010611
Mouse: B6.129S4-*Il2rg*^{tm1Wjl}/J	The Jackson Laboratory	JAX:003174
Mouse: *Aicda*^{tm1Hon}	Muramatsu et al., 2000	MGI: 2156156
Mouse: *Blimp1*$^{Gfp/+}$	Kallies et al., 2004	MGI: 3510704
Mouse: *Il4ra*$^{f/f}$	Herbert et al., 2004	N/A
Mouse: *Ccl19*$^{Cre/+}$	Chai et al., 2013	MGI: 5526991
Mouse: *CD21*$^{Cre/+}$	Kraus et al., 2004	MGI: 3047571

(*Continued on next page*)

Continued		
REAGENT or RESOURCE	SOURCE	IDENTIFIER
Mouse: *S1pr2*$^{CreERT2/+}$	Shinnakasu et al., 2016	MGI: 6435090
Mouse: *Stat6*$^{-/-}$	Takeda et al., 1996	MGI: 1888385
Mouse: *S1pr2*$^{Venus/+}$	Moriyama et al., 2014	N/A
Oligonucleotides		
Il4ra sgRNA 1 (5′-CAAAATCAGACAGCCCACAG-3′)	This paper	N/A
Il4ra sgRNA 2 (5′-GATGTAGTCAGAGAAGCAGG-3′)	This paper	N/A
Recombinant DNA		
pMCP-BFP	Kotov et al., 2019	N/A
Software and algorithms		
GraphPad Prism	GraphPad Software	http://www.graphpad.com/scientific-software/prism/ RRID: SCR_002798
Fiji	NIH	http://fiji.sc/ RRID: SCR_002285
R v3.6.2	R Foundation for Statistical Computing	https://www.r-project.org/
Cell Ranger v3.1.0	10x Genomics	https://support.10xgenomics.com/single-cell-gene-expression/software/pipelines/latest/what-is-cell-ranger RRID: SCR_017344
Seurat v3.1.1	Satija Lab	http://satijalab.org/seurat/ RRID: SCR_007322
Scanpy v1.4.6	Theis Lab	https://icb-scanpy.readthedocs-hosted.com/en/stable/ RRID: SCR_018139
ScVelo v0.1.25	Theis Lab	https://scvelo.readthedocs.io/index.html RRID: SCR_018168
Velocyto v0.17	velocyto-team	http://velocyto.org/ RRID: SCR_018167
LoomR v0.2.1.9	Satija Lab	https://github.com/mojaveazure/loomR
loompy v3.0	Linnarsson Lab	http://loompy.org/ RRID: SCR_016666
Monocle 2	Trapnell lab	http://cole-trapnell-lab.github.io/monocle-release/docs/ RRID: SCR_016339
VISION v1.1.0	Yosef Lab	https://yoseflab.github.io/VISION/news/index.html
IgBLAST V1.14.0	NCBI	https://ncbi.github.io/igblast/rel/Release-notes.html RRID: SCR_002873
Immcantation	Kleinstein Lab	https://immcantation.readthedocs.io/en/stable/index.html
Plotly Python Open Source Graphing Library v4.5.3	Plotly	https://github.com/plotly/plotly.py/ RRID: SCR_013991
RStudio	RStudio	https://www.rstudio.com/products/rstudio/ RRID: SCR_000432
GSEA v4 for Linux	GSEA team	https://www.gsea-msigdb.org/gsea/index.jsp RRID: SCR_003199
Weblogo 3	Crooks et al., 2004	http://weblogo.threeplusone.com/ RRID: SCR_010236
Flowjo	Treestar	https://www.flowjo.com/ RRID: SCR_008520

RESOURCE AVAILABILITY

Lead contact

Further information and requests for resources and reagents should be directed to and will be fulfilled by the lead contact, Jason Cyster (Jason.Cyster@ucsf.edu).

Materials availability

AS20-OVA generated in this study is available from the Lead Contact with a completed Materials Transfer Agreement.

Data and code availability

Single-cell RNA-seq data have been deposited at GEO (GSE180920).

This paper does not report original code.

Any additional information required to reanalyze the data reported in this paper is available from the lead contact upon request.

EXPERIMENTAL MODEL AND SUBJECT DETAILS

Mice

B6 (Jax 000664) and Boy/J (Jax 002014) were originally purchased from the Jackson Laboratory. B6 (NCI 556) and B6-Ly5 (NCI 564) mice were purchased from National Cancer Institute at age 6-8 weeks. *Il4ra*$^{-/-}$ mice (Jax 003514) and *Stat6*$^{-/-}$ mice on a B6 background were provided by Drs. Mark Ansel and Richard Locksley, respectively. Some *Il4ra*$^{-/-}$ mice developed severe dermatological lesions and poor health and were excluded from the study. IL-2Rγ-chain (Cγ) deficient mice (Jax 003174) were purchased form Jackson Laboratory. *S1pr2*$^{Venus/+}$ were generated as previously described (Moriyama et al., 2014). *Aicda*^{tm1Hon} (Muramatsu et al., 2000) and *Blimp1*$^{Gfp/+}$ *(Prdm1*$^{Gfp/+}$*)* mice (Kallies et al., 2004) were provided by Chris Allen. *Il4ra* floxed mice (Herbert et al., 2004) were provided by Mark Ansel. *Ccl19*$^{Cre/+}$ mice (Chai et al., 2013) and *CD21*$^{Cre/+}$ mice (Kraus et al., 2004) were from an internal colony. *Cas9*$^{f/f}$ (Rosa26-LSL-Cas9, 026175) and *Cγ1*$^{Cre/+}$ (010611) mice were from Jax. *S1pr2*$^{CreERT2/+}$ mice were provided by T. Okada at the RIKEN Center for Integrative Medical Sciences (Shinnakasu et al., 2016). All mice were maintained under specific-pathogen free conditions and used according to institutional and governmental guidelines for animal welfare.

METHOD DETAILS

Immunization and treatment

For various *in vivo* experiments, mice were given 50 μg NP-haptenated antigen (Biosearch Technology) plus 1 μg LPS in 50 μL aluminum hydroxide gel (Invivogen) by i.p. injection. NP_{28}-CGG, NP_{28}-KLH or NP_{32}-KLH was used in all experiments except in the *Il4ra*$^{-/-}$, *Cγ*$^{-/-}$ and *Ccl19-Cre Il4ra*$^{f/f}$ mice that were reconstituted with WT BM; in these chimeric mice NP_{14}-CGG was used. To boost the immunization, 25 μg soluble NP-haptenated antigen was given by i.v. injection. To induce Cre expression, 20mg/ml corn oil dissolved tamoxifen (Sigma–Aldrich) was injected at 2 mg per 20 g mouse i.p. at days 4, 6 and 8 post immunization. Normal chow was replaced with TAM diet (Envigo) on the day after the final tamoxifen dose.

Mixed or reverse bone marrow chimeras

For mixed chimeras, CD45.1 B6 mice were lethally irradiated by X-ray and transferred intravenously with BM cells mixed at a 1:1 ratio for WT CD45.1:WT CD45.2 control chimeras and a 2:3 ratio for WT CD45.1:*Il4ra*$^{-/-}$ CD45.2 chimeras. Typically we observed enhanced reconstitution of the follicular B cell compartment by *Il4ra*$^{-/-}$ BM such that the latter chimeras had on average 80% *Il4ra*$^{-/-}$ follicular B cells. For reverse chimeras, CD45.2 *Il4ra*$^{+/+}$ and *Il4ra*$^{-/-}$mice were lethally irradiated and transferred intravenously with CD45.1 B6 BM cells. Chimeras were immunized 6-8 weeks post reconstitution.

Retroviral constructs and transductions

Il4ra sgRNA sequences were selected using Benchling's CRISPR Guide tool. The following *Il4ra* sgRNA sequences were used: sgRNA 1 (5′-CAAAATCAGACAGCCCACAG-3′); sgRNA 2 (5′-GATGTAGTCAGAGAAGCAGG-3′). The tRNA-gRNA-tRNA pMIA plasmid was used as a template for generating the tRNA-gRNA arrays, and these arrays were cloned into a pMCP-BFP vector by golden gate cloning. The pMCP-BFP sgRNA vector was generated by digesting the pMCPA vector (Kotov et al., 2019) with NcoI and NotI to remove Ametrine and replace it with tagBFP by In-Fusion Cloning. Retrovirus was generated by transfecting the Plat-E packaging cell line with 7.5 μg plasmid DNA and 16 μL Lipofectamine 2000 (Thermo Fisher Scientific). *Cγ1*$^{Cre/+}$ *Cas9*$^{f/+}$ mice were treated with 3 mg 5-fluorouracil (Sigma–Aldrich) by i.v. injection. Bone marrow was collected after 4-5 days and cultured in complete DMEM containing 10% fetal bovine serum, antibiotics (penicillin (50 IU/ml) and streptomycin (50 mg/ml); Cellgro) and 10 mM HEPES (pH 7.2; Cellgro), supplemented with IL-3, IL-6 and stem cell factor. Bone marrow cells were spin-infected twice at days 1 and 2 and then transferred into irradiated recipients.

EdU labeling and analysis

For 1h labeling, following immunization, mice were given intravenously 0.5 mg EdU 1h before being sacrificed. For long term labeling, immunized mice were intravenously given 0.5 mg EdU every 4 hours for 3 times 11 days post immunization and analyzed 3 days after EdU labeling. Cells were stained for incorporated EdU with the Click-iT EdU Alexa Fluor 647 Flow Cytometry Assay Kit (Invitrogen), according to the manufacturer's instructions.

IL4 injection and analysis

2 μg mouse IL4 (PeproTech) and 10 μg anti-IL4 (clone 11B11, Bio X cell) were incubated at RT for 15min to make IL4-αIL4 complex. Immunized mice were intravenously given 2 μg complex once per day at day 11, 12, 13 post immunization, and analyzed at day 14.

AS20-OVA stimulation

The expressed Hc and Lc antibody genes in the CD45.1 specific AS20-1.17 hybridoma were sequenced. The Hc VDJ region was cloned into a vector (pBR322) containing the IgG1 constant regions coupled at the C terminus to chicken OVA or a peptide (aa 57-346) from the malaria circumsporozoite (CS) protein as a control (vectors kindly provided by Michel Nussenzweig); the light chain VJ region was cloned into a vector containing the kappa C1 constant region (Boscardin et al., 2006). The antibody conjugates were expressed in HEK293 cells and purified using protein G. Naive OT-II T cells were intravenously injected into B6 mice in combination with $CD45.1^+$ and $CD45.2^+$ MD4 B cells. Each recipient mouse was given 30 μg HEL-OVA antigen plus 1 μg LPS in alum (Thermo Scientific). 4-5 days post immunization, recipients were intravenously given 30 μg AS20-CS or AS20-OVA alone or with 100 μg anti-IL4 antibody (11B11) and analyzed 12 hours later.

Flow cytometry

Single-cell suspension of splenic cells were washed, blocked with 2.4G2 antibody (BioXcell), and stained with antibodies of indicated specificities in MACS buffer. Staining reagents include: BV786 anti-CD19 (1D3), PE-Cy7 anti-CD38 (90), Alexa Fluor 647 anti-CCR6 (140706), BV786 anti-B220 (RA3-6B2), BV421 anti-CD138 (281-2), BV711 anti-CD138 (281-2), PE-Cy7 anti-CD95 (Jo2), eFlour450 anti-GL7 (Ly-77), FITC anti-GL7 (Ly-77), PE-Cy7 anti-CD31 (MEC13.3), APC anti-CD23 (B3B4), PerCP/Cy5.5 anti-IgD (11-26c.2a), APC anti-Ki67 (16A8), BV605 anti-CD45.2 (104), BV605 anti-CD45.1 (A20) and BV605 anti-CD86 (GL-1) from Biolegend; biotinylated anti-CXCR4 (2B11), PE anti-CD31 (MEC 13.3), PE anti-IL4Ra (mIL4R-M1), Biotin anti-IL4Ra (mIL4R-M1), FITC anti-CD79b (HM79b), purified anti-CD72 b and c Alloantigens (JY/93), streptavidin-BV711 and streptavidin-BV605 from BD Biosciences; biotinylated anti-Ephrin-B1 polyclonal antibody from R&D System; NP-PE and NIP-BSA-biotin were used to stain for NP-binding cells (Biosearch Technology). Dead cell exclusion was based on Fixable Viability Dye eFluor 780 staining (eBioscience) and non-singlet events were excluded with FSC-W/FSC-H characteristics. For intracellular staining, cells were stained using Cytoperm/Cytofix kit (BD Biosciences) or Foxp3/Transcription Factor staining Buffer set (eBioscience) according to the manufacturer's protocol. All data were collected on an LSR II cytometer (BD) and analyzed with FlowJo software (TreeStar).

Immunofluorescent staining

Mesenteric lymph nodes were fixed in 4% paraformaldehyde in PBS for 4 hours on ice and incubated in 30% sucrose overnight, followed by embedding in tissue freezing medium (OCT). Cryosections of 10 μm were stained with goat anti-IgD, rabbit anti-Tmem119, APC-conjugated anti-CD21/35, biotin-conjugated EpCAM, streptavidin-PE (Biolegend) and AMCA-conjugated donkey anti-goat IgG (H+L) (Jackson Immunoresearch). Images were captured with a Zeiss AxioOberver Z1 inverted microscope.

Single cell sequencing and analysis

Two sets of 7-day and 14-day wild-type GC B cells were sorted from mice immunized as above. Single cells were captured using the 10X Chromium (10X Genomics), and libraries was prepared according the manufacturer's instructions (Chromium Single Cell 5′ Library & Gel Bead Kit, Chromium Single Cell 5′ Library Construction Kit, and Chromium Single Cell V(D)J Enrichment Kit, 10x Genomics). Libraries were run on the HiSeq4000 for Illumina sequencing. Sequencing data were processed with the 10X Cell Ranger (10X Genomics). Seurat (v3) was used for the further analysis. For day 7, sample 1 mean reads per cell was 314,827 and sample 2 was 565,017. Median genes per cell of sample 1 was 4213 and sample 2 was 4118. For day 14, sample 1 mean reads per cell was 82,769 and sample 2 was 96,660. Median genes per cell of sample 1 was 1590 and for sample 2 was 1456. Cells expressing less than 200 genes were filtered out. Cells with the percentage of mitochondrial genes per cell less than 5% were used for the day 7 dataset; due to the lower read depth in the day 14 dataset, cells with the percentage of mitochondrial genes per cell 20% were used. Cells with the frequency of ribosome genes per cell more than 30% were filtered out. 3542 (1012+2530) cells from the day 7 group and 19757 (9109+10648) cells from the day 14 group remained for further analyzed. We used ''LogNormalize'' (scale factor: 10,000) to normalize gene expression in each cell. The influence of batch effects and percentage of mitochondrial genes in each group/condition were regressed out using Seurat. The top 2000 variable genes of each group were selected for the PCA analysis. According to the PCElbowPlot, we chose the first 30 principal components (PCs) for the UMAP dimension reduction and clustering (resolution is 0.4). The cell markers of different clusters were identified using the FindAllMarkers function. Cell cycle score and classification were calculated by CellCycleScoring function based on the expression of G2/M and S phase markers (Kowalczyk et al., 2015). We used the published list of genes (Milpied et al., 2018; Victora et al., 2012) to calculate the DZ and LZ scores with the AddModuleScore function from the Seurat package. A post GC B cell RNA sequencing dataset (Laidlaw et al., 2017) was used to calculated the post GC B cell gene set signature with DESeq2. Log2 fold change more than 0.3 and adjusted p value less than 0.001 genes were used as the post GC B cell gene set signature (Table S2). Gene set signature score were calculated with VISION (DeTomaso et al., 2019) on the Seurat object.

The pseudo time analysis on $CD23^+$ LZ GC B cell were carried out with Monocle v2 (Qiu et al., 2017). Top 1000 marker genes for each cluster were used for unsupervised ordering of the cells and the DDRTree algorithm implemented in Monocle2 was applied for trajectory reconstruction. Branch specific genes were calculated by the BEAM algorithm. Genes with q value less than 0.001 were plotted and used for GSEA analysis. To determine the fate of each branch, we compared the branch specific genes with the q value less than 0.001 to the published RNA sequencing datasets (Ise et al., 2018; Laidlaw et al., 2017; Shinnakasu et al., 2016) using GSEA.

For RNA velocity analysis, the spliced reads and unspliced reads were recounted by the Velocyto package (La Manno et al., 2018). We calculated the RNA velocity values for each gene each cell and embedded the RNA velocity vector to low-dimension space

following the scVelo pipeline. The RNA velocity graph based pseudo time was calculated by Velocity pseudotime function from scVelo (Bergen et al., 2020).

BCR sequence reads were processed using Cell Ranger V3. AssignGenes and MakeDb python scripts were used to process 10X V(D)J data and generate a Change-O format file. ParseDb python script was used to parse the output file into heavy chain Change-O file. Only the record from which the barcode was detected and that passed the quality control for 5′ gene expression analysis was kept and merged to the Seurat object as meta information. $CD23^{+}$ LZ GC B cells were grouped into pre-memory B cell and pre-plasma cell according the pseudotime analysis, and the cell expressing IGHV1-72*01 were kept. The CDR1 sequence of each cell in each group was used to generate the sequence logo by the WebLogo V3 (Crooks et al., 2004).

To determine the difference between control and stromal cell IL4ra-deficient mice, we sorted GC B cells from four mice and pooled them together in each condition. For the control sample, mean reads per cell was 25534, median genes per cell was 1727. For the stromal cell IL4Ra deficient sample, mean reads per cell was 28062, median genes per cell was 1791. Naive B cells, non-B cells and low-quality cells were removed first. Cells expressing less than 200 genes were filtered out. Cells with a percentage of mitochondrial genes more than 10% were removed. 8038 cells were left in the control group and 7314 cells were left in the stromal cell IL4Ra-deficient group. Count data was normalized to log scale. The top 2000 variable genes of each group were selected. Two datasets were integrated with Seurat by using CCA based method. Clustering was carried out with this integrated dataset. For the BCR heavy chain analysis, the same preprocessing was carried out as described above. If the cell barcode was detected by more than one sequence only one was kept. Only functional sequences were used for analysis. 7791 heavy chain sequences were left in the control group and 8419 heavy chain sequences were left in the in the stromal cell IL4Ra-deficient group. BCR sequences in which the barcode was also detected and kept in the gene expression dataset were kept and mapped into Seurat object as meta information.

QUANTIFICATION AND STATISTICAL ANALYSIS

Statistics and graphing were done with Prism (GraphPad). Two-tailed Student's t tests were used to compare endpoint means of different groups unless otherwise indicated.